

Comparison of Na_2SO_4 , K_2SO_4 and $\text{Na}_2\text{SO}_4\text{-K}_2\text{SO}_4$ deposit induced hot corrosion of a $\beta\text{-NiAl}$ coating

Yaping Wang, Rishi Pillai, Elena Yazhenskikh, Martin Frommherz, Michael Müller,

Willem Joseph Quadackers, Dmitry Naumenko

Highlights:

- The rate and morphology of type II hot corrosion attack strongly affected by p_{SO_3} and deposit composition
- K_2SO_4 and $\text{Na}_2\text{SO}_4\text{-K}_2\text{SO}_4$ deposits are more corrosive than Na_2SO_4 .
- The formation of Ni-containing mixed sulphate phases and liquid phases in the presence of K_2SO_4 accelerate the corrosion attack
- Stability diagrams of the $\text{Na}_2\text{SO}_4\text{-K}_2\text{SO}_4\text{-NiO-SO}_3$ system were calculated using an in-house developed thermodynamic database
- The calculated stability diagrams agree well with the hot corrosion results

Comparison of Na₂SO₄, K₂SO₄ and Na₂SO₄-K₂SO₄ deposit induced hot corrosion of a β-NiAl coating

Yaping Wang ^{a,*}, Rishi Pillai ^{a,b}, Elena Yazhenskikh ^a, Martin Frommherz ^c,

Michael Müller ^a, Willem Joseph Quadackers ^a, Dmitry Naumenko ^a

^a Forschungszentrum Juelich, Institute of Energy and Climate Research (IEK-2),

Wilhelm-Johnen-Straße, 52428 Juelich, Germany

^b Oak Ridge National Laboratory, Materials Science and Technology Division, Oak

Ridge, Tennessee, 37831, USA (present address)

^c MTU Aero Engines AG, Dachauer Strasse 665, 80995 München, Germany

* Corresponding author, e-mail address: ya.wang@fz-juelich.de

Abstract:

Hot corrosion behaviour of a β-NiAl coating induced by Na₂SO₄, K₂SO₄, and Na₂SO₄-K₂SO₄ deposits was investigated at 700 °C in air + 300 ppm SO₂. To provide an insight into the corrosion mechanisms, phase equilibria of the Na₂SO₄-K₂SO₄-NiO-SO₃ system were calculated using an in-house developed thermodynamic database. The attack rates and morphologies could be correlated with the deposit compositions and their reactions with oxides. K₂SO₄ and Na₂SO₄-K₂SO₄ deposits are more corrosive than Na₂SO₄. This is attributed to a reduction of the melting temperature of the deposit and the formation of Ni-containing mixed sulphate phases in the presence of K₂SO₄.

Keywords: Molten salts (A); Nickel (A); Metal coatings (A); Modelling studies (B); SEM (B); Hot corrosion (C)

1. Introduction

High-temperature components in gas-turbines are frequently exposed to sulphur-containing gases and alkali sulphate deposits during service. The deposit-induced accelerated corrosion attack termed hot corrosion may result in rapid degradation and failure of the turbine components [1, 2]. Hot corrosion studies of the involved materials (Ni-based alloys and coatings) are thus of significant importance for understanding the mechanisms, identifying ways to mitigate the attack and extending the life span of the components. Hot corrosion attack is commonly categorized as high-temperature (type I) and low-temperature (type II) corrosion [3]. After decades of investigation, it is generally agreed that formation of liquid phase is a pre-requisite for the occurrence of severe low-temperature hot corrosion [4]. Na_2SO_4 commonly found in the deposit on the surface of components is proved to be detrimental because of the low-temperature eutectic reactions with sulphates produced from the oxides of alloying elements and SO_3 , in particular NiSO_4 and CoSO_4 . The relevant mechanisms have been extensively studied and described in review papers as well as textbooks [3-8].

Apart from Na_2SO_4 , K_2SO_4 is frequently detected in the deposits [9, 10]. Similar to Na_2SO_4 , K_2SO_4 forms a low melting temperature eutectic with CoSO_4 (m. p. = 538 °C [11]) and $\text{Fe}_2(\text{SO}_4)_3$ (m. p. = 627 °C [12]). The addition of K_2SO_4 to Na_2SO_4 has been reported to increase the hot corrosion rates in Co and Fe based alloy systems,

by further decreasing the melting temperature of the salt due to ternary eutectic reactions [11, 12]. $\text{Na}_2\text{SO}_4\text{-K}_2\text{SO}_4$ mixtures were typically used as deposits for hot corrosion studies of Ni-based alloys, but the focus of these studies was either the fatigue mechanisms [13, 14] or the comparison between isothermal and cyclic hot corrosion [15]. Hot corrosion mechanisms of Ni-based alloys and coatings related to K_2SO_4 containing deposits, particularly the role of K_2SO_4 addition have, as far as known to the authors, hardly been elucidated.

In the present study, the corrosion reactions induced by Na_2SO_4 , K_2SO_4 , and binary $\text{Na}_2\text{SO}_4\text{-K}_2\text{SO}_4$ mixture deposits were compared by performing a series of hot corrosion tests in air + 300 ppm SO_2 using a $\beta\text{-NiAl}$ coating on a single-crystal Ni-based superalloy. Apart from the hot corrosion experiments, various mixtures of alkali sulphates and Ni-oxide/sulphate powders were prepared and exposed under the same experimental conditions as the coated specimens. Comparison of the composition and morphologies of reaction products between the coated superalloy and mixed sulphate powders allowed a better understanding of the underlying corrosion phenomena. The stability diagrams of the $\text{Na}_2\text{SO}_4\text{-K}_2\text{SO}_4\text{-NiO-SO}_3$ system were calculated using an in-house developed thermodynamic database. Based on the experimental and calculation results, the mechanisms of hot corrosion attack caused by different alkali salts will be extensively discussed.

2. Material and methods

2.1 Materials

An aluminide coating on the Ni-based single-crystal superalloy PWA1484 was used in the present study. The chemical composition of the PWA 1484 batch used was measured in our previous work [16] by inductively coupled plasma optical emission spectroscopy (ICP-OES) with a relative error of up to 10% and the result of the analysis is provided in Table 1. An industrially employed chemical vapor deposition (CVD) process with a low Al activity pack was used for aluminizing. The coating thickness is around 60 μm . Based on the observed morphologies, the coating can be divided into two parts, namely the outer coating and the interdiffusion zone (IDZ), as shown in our previous work [16]. The outer coating of about 30 μm in thickness consists of β -NiAl with a composition of approximately Ni-41 at. % Al-6 at.% Co-2 at.% Cr.

Table 1 The composition of the as-received Ni-based single-crystal superalloy PWA 1484 in wt. % determined by ICP-OES [16]

Element	Co	Cr	Al	Ta	W	Mo	Re	Hf	Ni
Concentration	9.91	4.85	5.63	9.0	6.0	2.0	3.0	0.1	Bal.

2.2 Experimental methods

2.2.1 Hot corrosion tests

Pure Na_2SO_4 , pure K_2SO_4 , and Na_2SO_4 -20 mol.% K_2SO_4 (Na_2SO_4 -20 K_2SO_4) mixture were used as deposits for the hot corrosion tests. To produce a deposit slurry,

82 wt. % dry salt powder was mixed with a special solvent, which consisted of 95 wt. % terpineol and 5 wt. % ethyl cellulose. Before corrosion tests, the slurry was applied to one surface of the specimens by painting. The painted specimens were then dried at 60 °C for 12 h. Assuming all terpineol evaporated during drying, the final composition of the deposit was 99 wt. % salt mixture + 1 wt. % cellulose. The amount of the deposit on the sample surface was measured to be around 30 mg / cm².

Rectangular coupon specimens with a size of 20×10×2 mm³ were used for hot corrosion tests. Prior to testing, the specimens with salt deposits were placed into alumina crucibles and subsequently exposed in a horizontally arranged tube furnace for 24 or 100 h. In all experiments, synthetic air-300 ppm SO₂ was used as the test atmosphere. A platinum honeycomb in front of the specimens was used to catalyse the reaction between O₂ and SO₂ for SO₃ production, and thereby to establish the equilibrium gas composition [17, 18]. The heating and cooling rates for the furnace operation during the hot corrosion tests were 10 °C/min and 2 °C/min, respectively.

2.2.2 Metallographic analysis

After exposure, metallographic cross-sections of the specimens were prepared using an oil-based solution to preserve any water-soluble species. Scanning Electron Microscopy (SEM) and Energy Dispersive X-Ray Analysis (EDX) were used for the observation of corrosion attack morphologies and measurements of the elemental distribution, respectively.

2.2.3 X-ray diffraction (XRD)

XRD measurements were conducted for identifying the phase structures of the alkali sulphate-Ni oxide/sulphate mixtures. An Empyrean diffractometer (Malvern Panalytical) with Cu-K α radiation (40 kV, 40 mA) and a PIXcel3D detector was used. The inorganic crystal structure database (ICSD, FIZ Karlsruhe) [19] and the powder diffraction file (PDF-2) [20] from the International Centre for Diffraction Data (ICDD) were used for the phase identification.

3. Experimental results

3.1 Hot corrosion morphologies after 24 h exposure

A series of hot corrosion tests with no deposit, pure Na₂SO₄, pure K₂SO₄, and Na₂SO₄-20K₂SO₄ mixture as deposits were performed at 700 °C in air + 300 ppm SO₂ for 24 h. The cross-sections of the post-test specimens were subsequently characterized using SEM-EDX. The corresponding backscatter electron (BSE) images are presented in Fig. 1a-d. After 24 h exposure, no significant attack was found in the salt-free specimen (Fig. 1a). For the specimen with Na₂SO₄, sparsely distributed pits were observed at the interface between the salt deposit and the coating (Fig. 1b). With K₂SO₄ deposit a relatively uniform corrosion attack of the coating was observed (Fig. 1c). About 30 % of the outer coating was reacted. With Na₂SO₄-K₂SO₄ deposit substantial coating corrosion occurred (Fig. 1d), whereby the corrosion pits locally reached the interdiffusion zone.

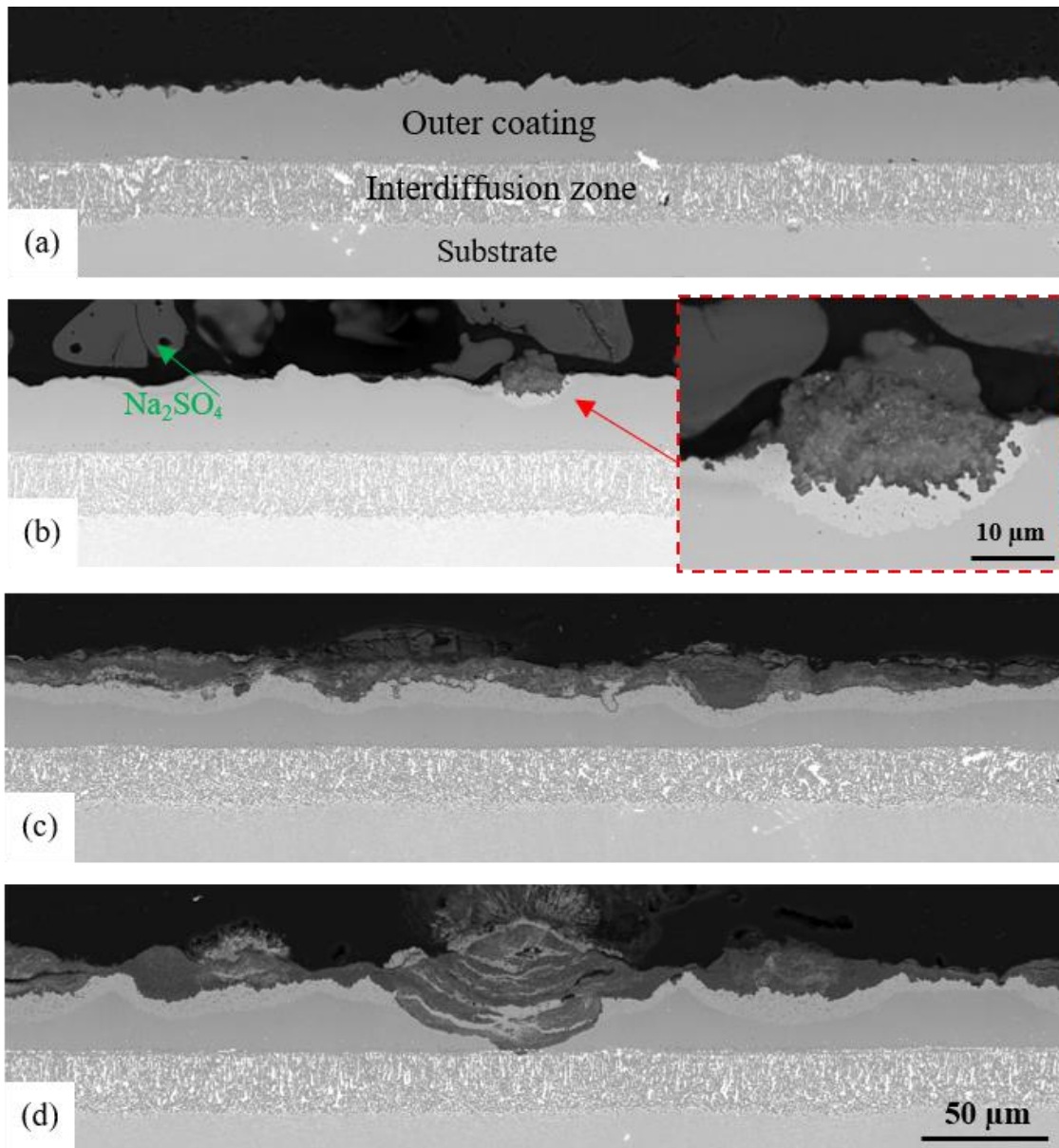


Fig. 1 SEM-BSE images of cross-sections of studied β -NiAl coating on Ni-base superalloy after hot-corrosion testing at 700 °C in air-300 ppm SO_2 for 24 h with (a) no deposit; (b) Na_2SO_4 ; (c) K_2SO_4 ; (d) Na_2SO_4 -20 K_2SO_4

Fig. 2 shows a detailed morphology and composition of the local corrosion pit formed after exposure of the coated alloy under Na_2SO_4 . According to the presented EDX-maps the pit contains mainly Al-rich oxides but also substantial amounts of Ni and sulphur. In the Al-depleted coating region below the pit, very fine S-rich

precipitates were observed, which were identified by EDX-analysis to be Cr-rich sulphides (not shown here, reported in [21]).

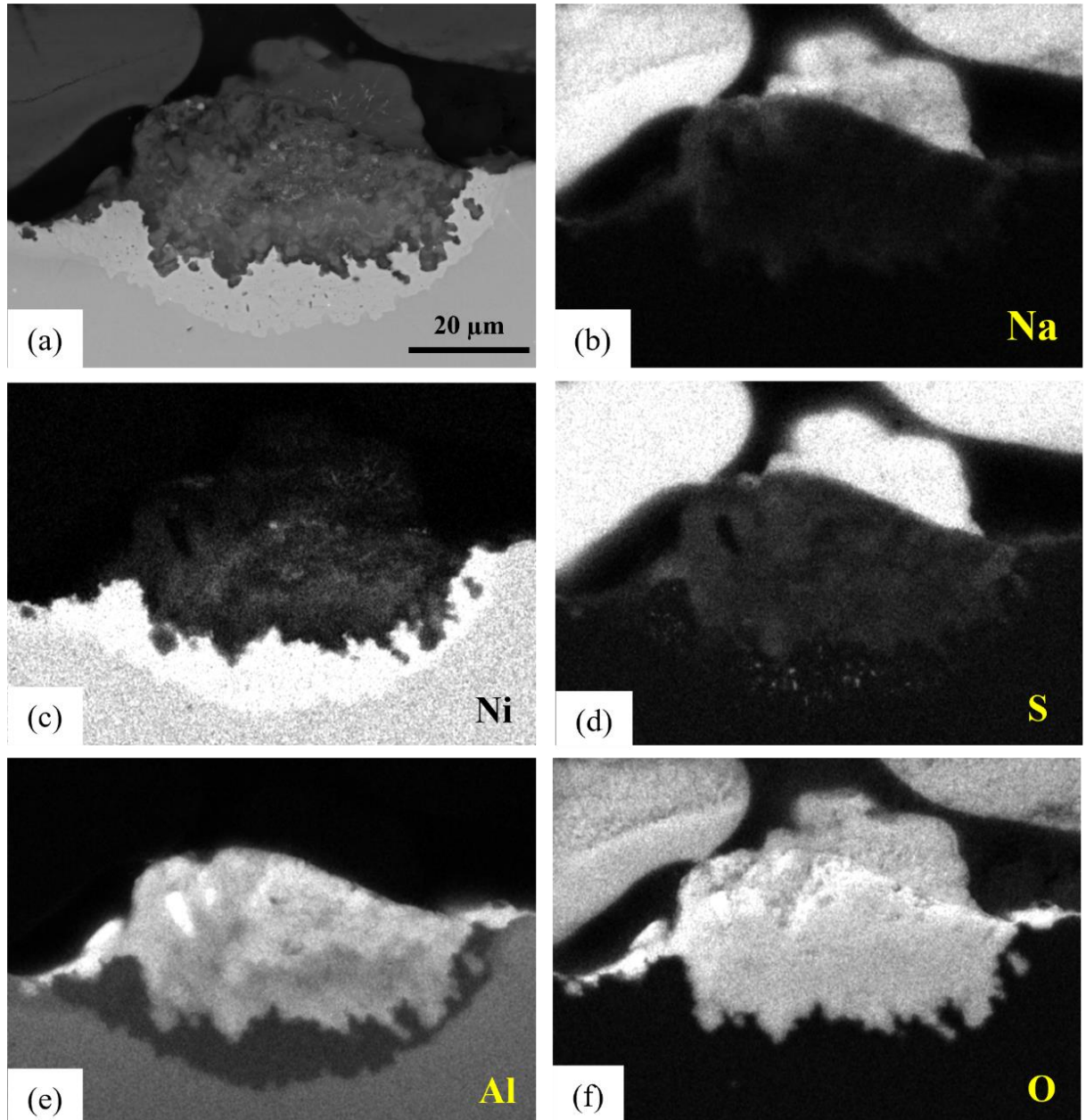


Fig. 2 (a) SEM-BSE image and (b)-(f) corresponding EDX-elemental maps of cross-section of studied β -NiAl coating on Ni-base superalloy after hot-corrosion testing with Na_2SO_4 deposit at 700 °C in air-300 ppm SO_2 for 24 h

A rather uniform layer of corrosion products was found in the specimen with K_2SO_4 deposit (Fig. 3). Based on comparison of the EDX-maps, this layer is presumably composed of Ni and Al rich oxides infiltrated with K_2SO_4 . In the lower part of the layer, Ni-sulphide precipitates were recognized that are marked by the yellow arrows in Fig. 3. Beneath the corroded layer an Al depleted coating was observed (Fig. 3d), in which fine sulphur-rich precipitates were dispersed. Based on the EDX analysis the Al-depleted zone consists of Ni_3Al . Quantitative EDX-analysis of the sulphur-rich precipitates was not possible due to their small size. Based on the EDX-results with unary Na_2SO_4 deposit (compare with Fig. 2) as well as exposures of NiAl coating with $Na_2SO_4-20K_2SO_4$ in our previous work [21] these particles are most likely Cr-sulphides.

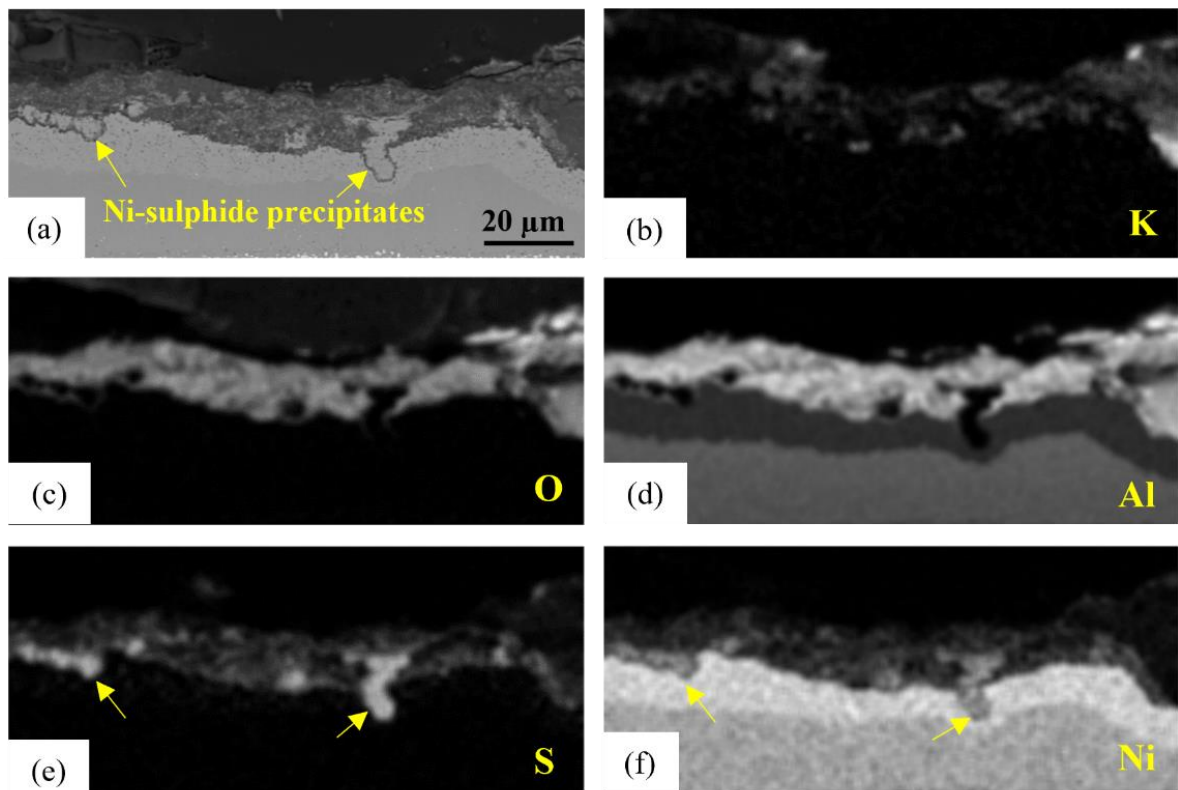


Fig. 3 (a) SEM-BSE image and (b)-(f) corresponding EDX-elemental maps of cross-section of studied β -NiAl coating on Ni-base superalloy after hot-corrosion testing with K_2SO_4 at 700 °C in air-300 ppm SO_2 for 24 h

The specimen with Na_2SO_4 -20 K_2SO_4 deposit underwent more severe hot corrosion attack during 24 h exposure than in case of the exposures with solely Na- or K-sulphate, resulting in a multiphase corrosion layer (Fig. 1d). Clearly, the addition of 20% K_2SO_4 to Na_2SO_4 aggravated the attack. To identify the corrosion products, the elemental distributions were analysed using EDX and the results are presented in Fig. 4. Al-rich oxides infiltrated with the salts were found to be the predominant corrosion products. At some locations where the attack was most severe, e.g. Zone A in Fig. 4a, the oxide layer evolved to multi-layers of Al-rich oxides interposed with NiO layers. Similar to the specimen with pure K_2SO_4 , Ni-sulphide bands were also found at the bottom part of the corrosion products in Zone A.

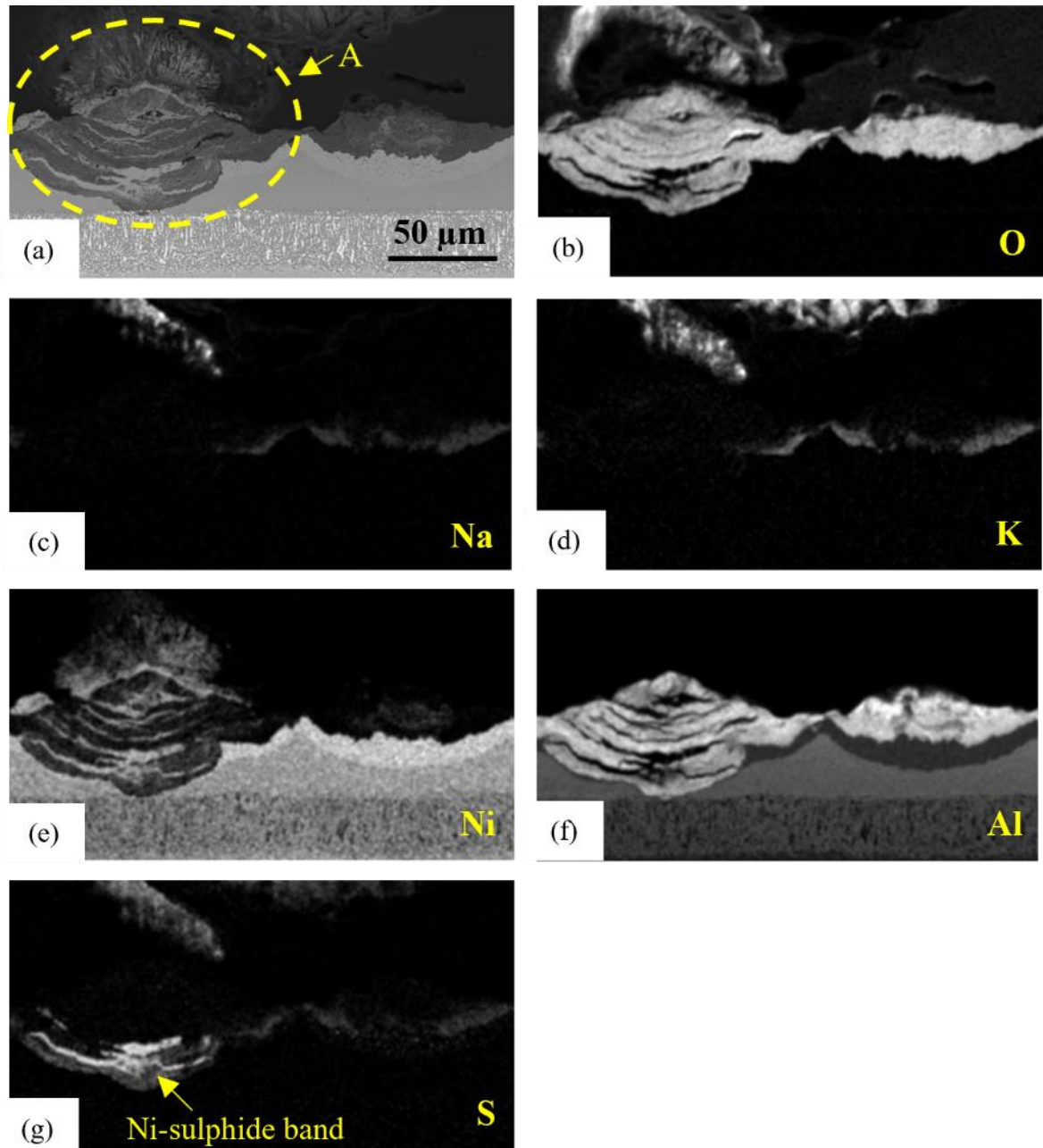


Fig. 4 (a) SEM-BSE image (area A marked by the circle is one location, where the attack was most severe) and (b)-(g) corresponding EDX-elemental maps of cross-section of studied β -NiAl coating on Ni-base superalloy after hot-corrosion testing with $\text{Na}_2\text{SO}_4\text{-}20\text{K}_2\text{SO}_4$ deposit at $700\text{ }^\circ\text{C}$ in air-300 ppm SO_2 for 24 h.

The morphology of the $\text{Na}_2\text{SO}_4\text{-}20\text{K}_2\text{SO}_4$ deposit on top of the $\beta\text{-NiAl}$ coating after 24 h exposure is presented in Fig. 5. The salt particles exhibit a dark phase (marked by A) and a relatively bright phase (marked by B). Some needle-like precipitates are also observed (marked by the yellow arrows, designated as phase C). A detailed explanation regarding this morphology will be given in Section 5.3.

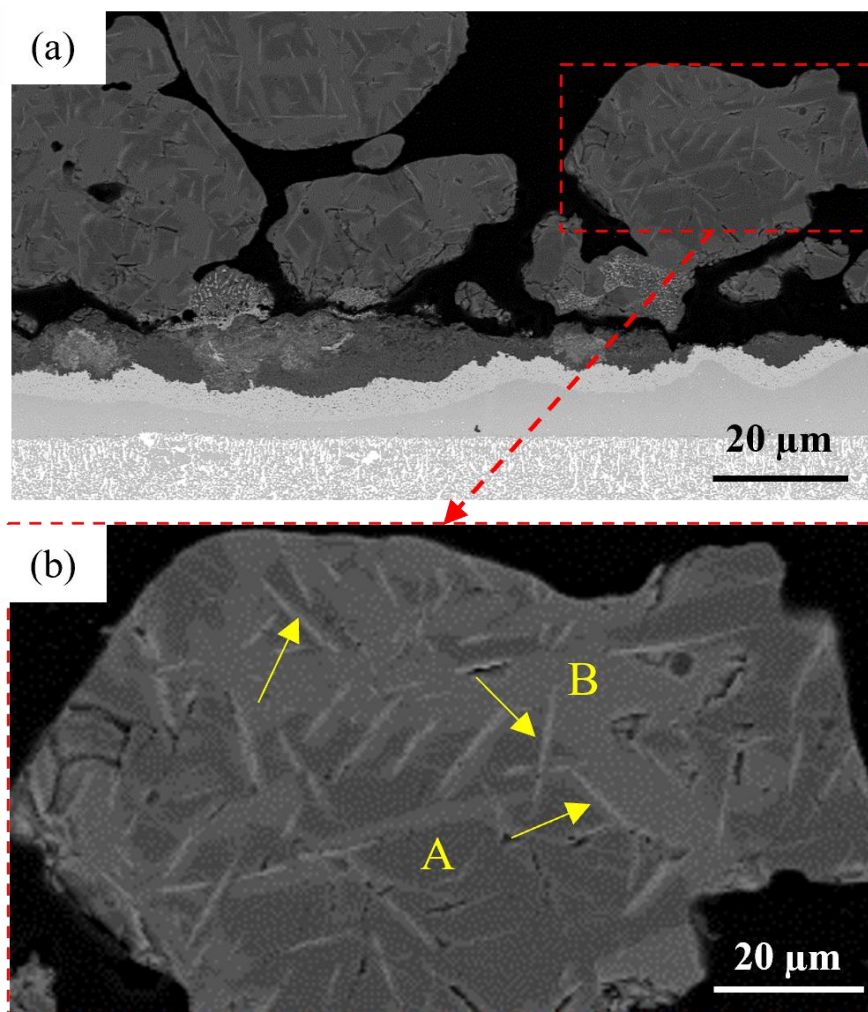


Fig. 5 (a) SEM-BSE image of cross-sections of studied $\beta\text{-NiAl}$ coating on Ni-base superalloy after hot-corrosion testing with $\text{Na}_2\text{SO}_4\text{-}20\text{K}_2\text{SO}_4$ deposit at 700 °C in air-300 ppm SO_2 for 24 h; (b) SEM-BSE image with a higher magnification of right upper part in (a) as marked by the

red dashed box. A and B in (b) represent a dark phase and a relatively bright phase in the salt particles, respectively. The arrows in (b) illustrate the needle-like precipitates. The phase compositions of the phases are provided in detail in section 3.1.

3.2 Hot corrosion morphologies after 100 h exposure

It is found from the macro-images of the exposed specimens (Fig. 6) that with K_2SO_4 and Na_2SO_4 - K_2SO_4 deposits the corrosion attack is more severe compared to that with Na_2SO_4 . In the latter case, white crystals of solid Na_2SO_4 can still be found on the specimen surface after exposure (Fig. 6a), whereas both K_2SO_4 containing deposits (Fig. 6b and c) feature pinkish and greenish reaction products. Although an unequivocal analysis appeared to be difficult, the pink and green products might be $CoSO_4$ [18] and NiO , respectively.

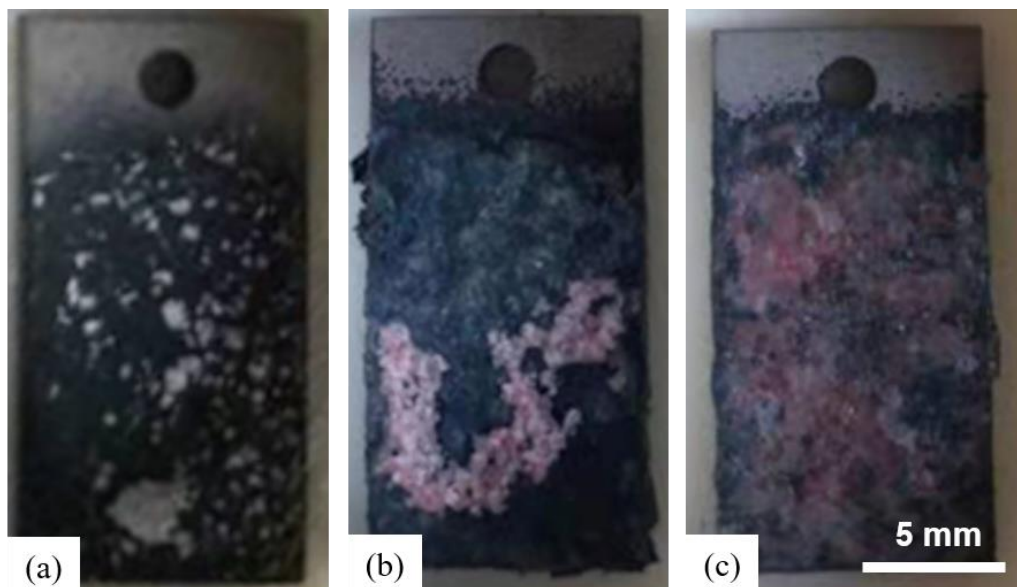


Fig. 6 Macro-images of studied β -NiAl coating on Ni-base superalloy after exposure at 700 °C for 100 h in air + 300 ppm SO_2 with (a) Na_2SO_4 ; (b) K_2SO_4 ; (c) Na_2SO_4 -20 K_2SO_4

The cross-sectional BSE images (Fig. 7) show that the differences in the hot corrosion morphology and its severeness among the three salts observed after 100 h exposure are qualitatively similar to those found after 24 h (compare with Fig. 1). For the specimen with Na_2SO_4 deposit a rather homogeneous corrosion attack was found (Fig. 7a-c). In the specimen with K_2SO_4 deposit, a thick mixed salt-oxide zone was observed. Underneath there was an irregular corrosion zone whereby its front locally reached the IDZ (Fig. 7d-f). The specimen with the binary salt mixture kept the major morphology characteristics of the short-term exposure, namely multiple Al-rich oxide layers with Ni oxide/sulphide bands within it (Fig. 7g-i). The front of the attack entered the IDZ (Fig. 7g). The results confirm the observations of the 24 h exposures that for the studied NiAl coating, the hot corrosion attack with K_2SO_4 and $\text{Na}_2\text{SO}_4\text{-}20\text{K}_2\text{SO}_4$ deposits is more severe than that with Na_2SO_4 deposit.

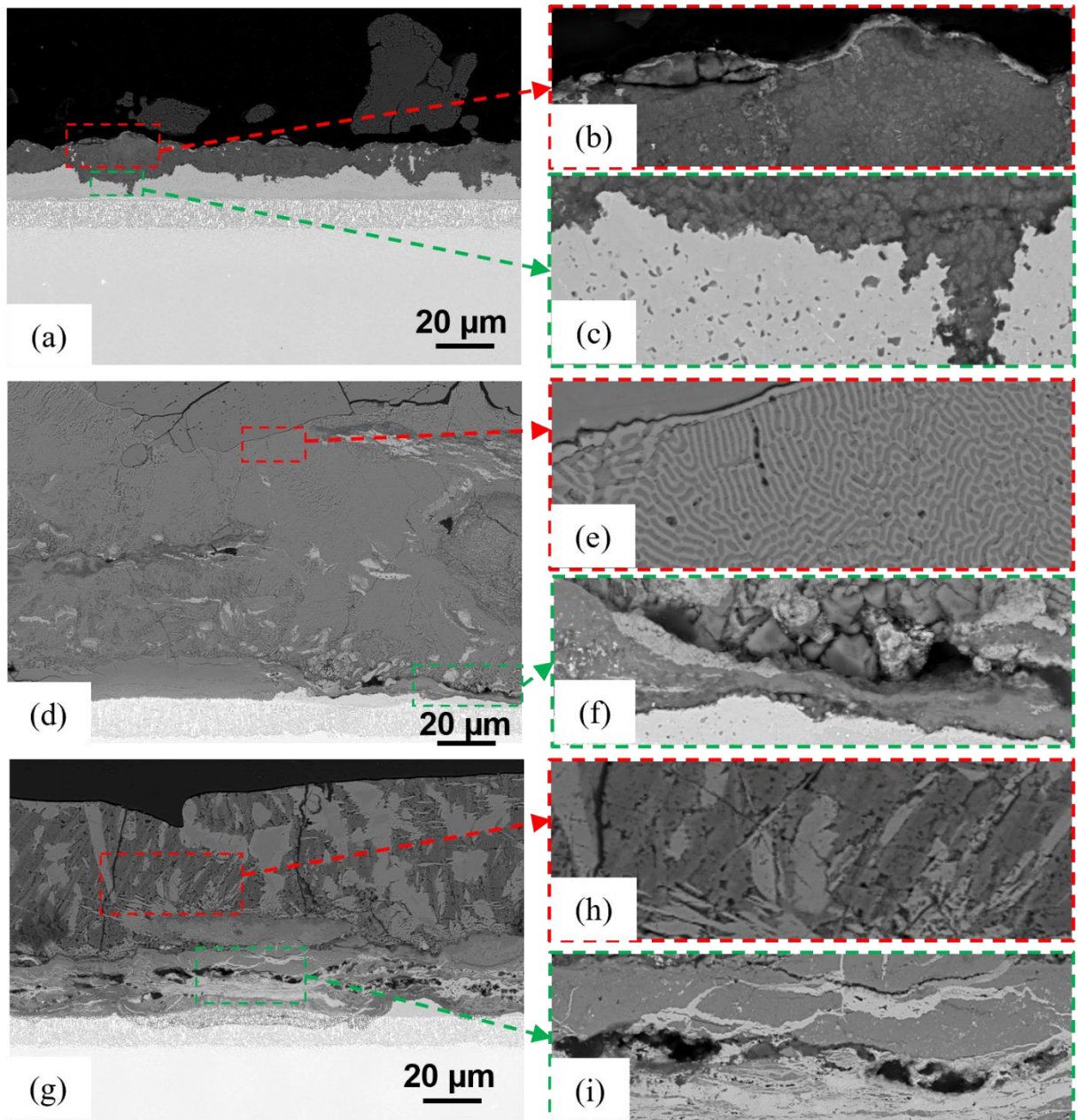


Fig. 7 BSE images of cross-sections of studied β -NiAl coating on Ni-base superalloy after hot-corrosion testing at 700 °C in air-300 ppm SO_2 for 100 h with: (a) (b) (c) Na_2SO_4 ; (d) (e) (f) K_2SO_4 ; (g) (h) (i) Na_2SO_4 -20 K_2SO_4 deposits

To identify the corrosion products, the specimens after 100 h exposure were examined using EDX, and the EDX-maps obtained are displayed in Fig. 8-Fig. 12. As shown in Fig. 8, with pure Na_2SO_4 a porous Al-rich oxide layer penetrated by Na_2SO_4

was observed as the major attack morphology. An Al depleted zone formed beneath the corroded layer (Fig. 8d). This depletion zone contained small sulphide particles (Fig. 8f). From the Cr distribution it is likely that these particles are Cr sulphides (Fig. 8h). Since only local pits were found after 24 h exposure with Na₂SO₄ (Fig. 1b), whereas a relatively thick corroded layer formed after 100 h exposure, apparently the incubation time of the corrosion reaction in this case is longer than that with K₂SO₄ and with the binary alkali salt deposits.

To better understand the reactions between the salts and the coating, the composition of the deposit after exposure was also studied. For the specimen coated with Na₂SO₄ salt the majority of the deposit fell off during the cross-section preparation (Fig. 6). Only some individual deposit particles were available for subsequent SEM analysis (Fig. 7a). The deposit particles appeared to consist mainly of Na₂SO₄. Around 1 at.% Ni was detected in the salt particles by EDX point analyses.

Interestingly, the reaction product of the K₂SO₄ deposit exhibited a lamellar microstructure (Fig. 7e and Fig. 9). Comparing Ni, Co, K, S and O EDX-maps in Fig. 9 reveals a laminated K-Ni (Co) distribution, whereas oxygen and sulphur are distributed relatively homogeneously (Fig. 9b and h). Since the distributions of Co (Fig. 9e) and Ni (Fig. 9d) are comparable, Co probably plays a similar role as Ni during the corrosion reaction. The compositions of two locations in Fig. 9a representing the K-Ni (Co) (spectrum 1) and K-rich (spectrum 2) phases were quantified using EDX analysis and the corresponding results are shown in Table 2. The phases marked by 1 and 2 in

Fig. 9a matches approximately with the stoichiometry of $K_2Ni_2(SO_4)_3$ and K_2SO_4 , respectively, assuming that Ni in the $K_2Ni_2(SO_4)_3$ phase is partially replaced by Co.

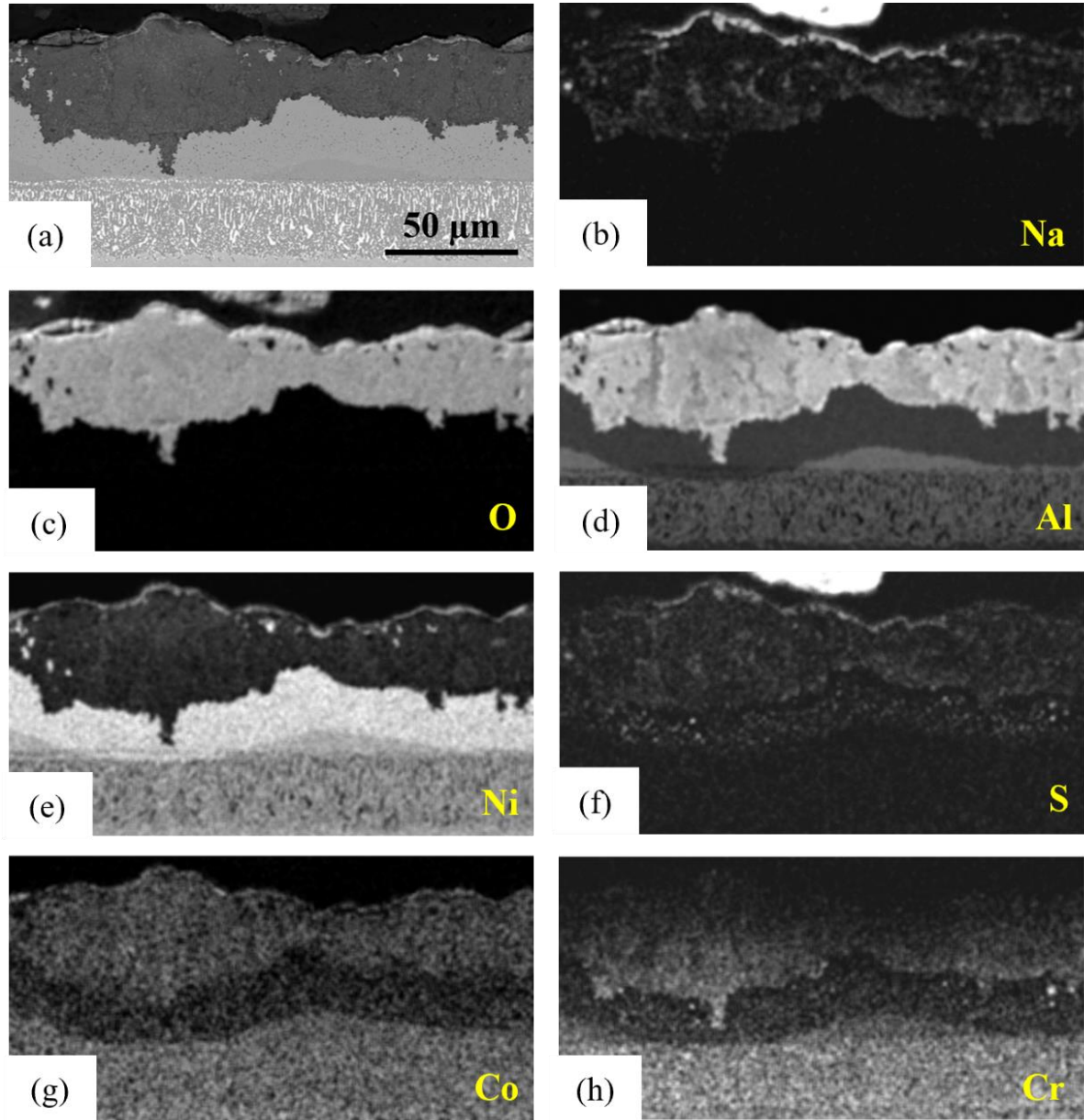


Fig. 8 (a) SEM-BSE image and (b)-(h) corresponding EDX-elemental maps of cross-section of studied β -NiAl coating on Ni-base superalloy after hot-corrosion testing with Na_2SO_4 at 700 °C in air-300 ppm SO_2 for 100 h

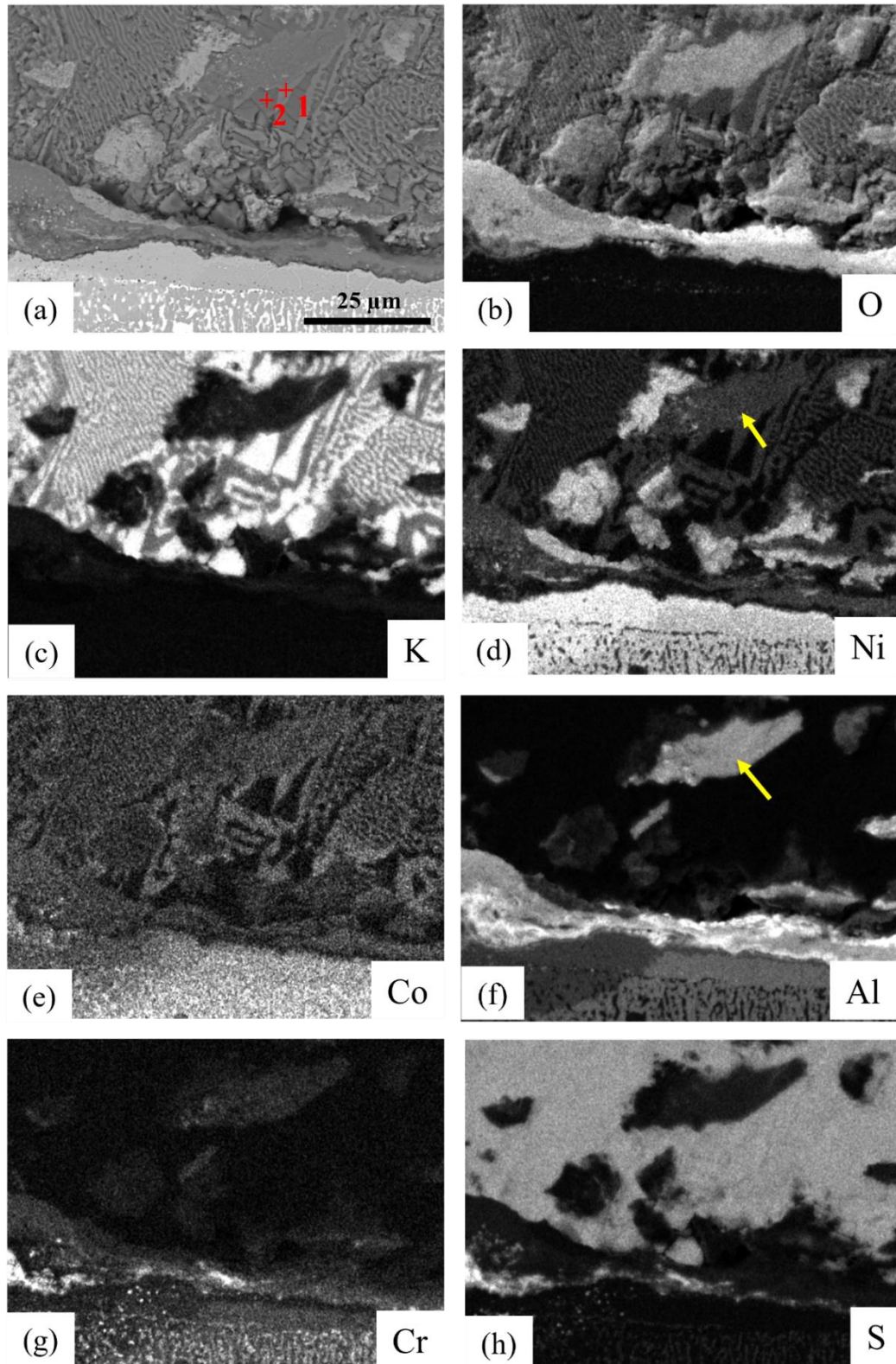


Fig. 9 (a) SEM-BSE image and (b)-(h) corresponding EDX-elemental maps of cross-section of studied β -NiAl coating on Ni-base superalloy after hot-corrosion testing with K_2SO_4 at 700 °C

in air-300 ppm SO₂ for 100 h. The compositions of the areas marked by 1 and 2 are shown in Table 2. The phase designated by the yellow arrows is a Ni, Al mixed oxide, e.g. NiAl₂O₄ spinel

Table 2 EDX point analysis of element concentrations of the reaction products in Fig. 9a (at. %)

Spectrum	O	Al	S	K	Ni	Co
1	63.0	0.3	15.7	10.9	7.5	2.7
2	57.5	-	14.4	27.8	0.4	-

The distribution of Al after the exposure with K₂SO₄ is completely different from that observed after exposure with pure Na₂SO₄. For the specimen with K₂SO₄, a relatively thin Al rich oxide layer formed at the interface between the salt and the remaining coating, as can be seen from Fig. 9 and Fig. 10. S-rich precipitates were found beneath the Al₂O₃ (Fig. 9h, Fig. 10f). Some Al₂O₃ layers can be seen as embedded islands within the deposited salt (Fig. 10d). Besides, an overlapping of Ni, Al and O was noticed in some locations (e.g. those marked by yellow arrows in Fig. 9d and f), which indicates the existence of a mixed oxide e.g. NiAl₂O₄ spinel.

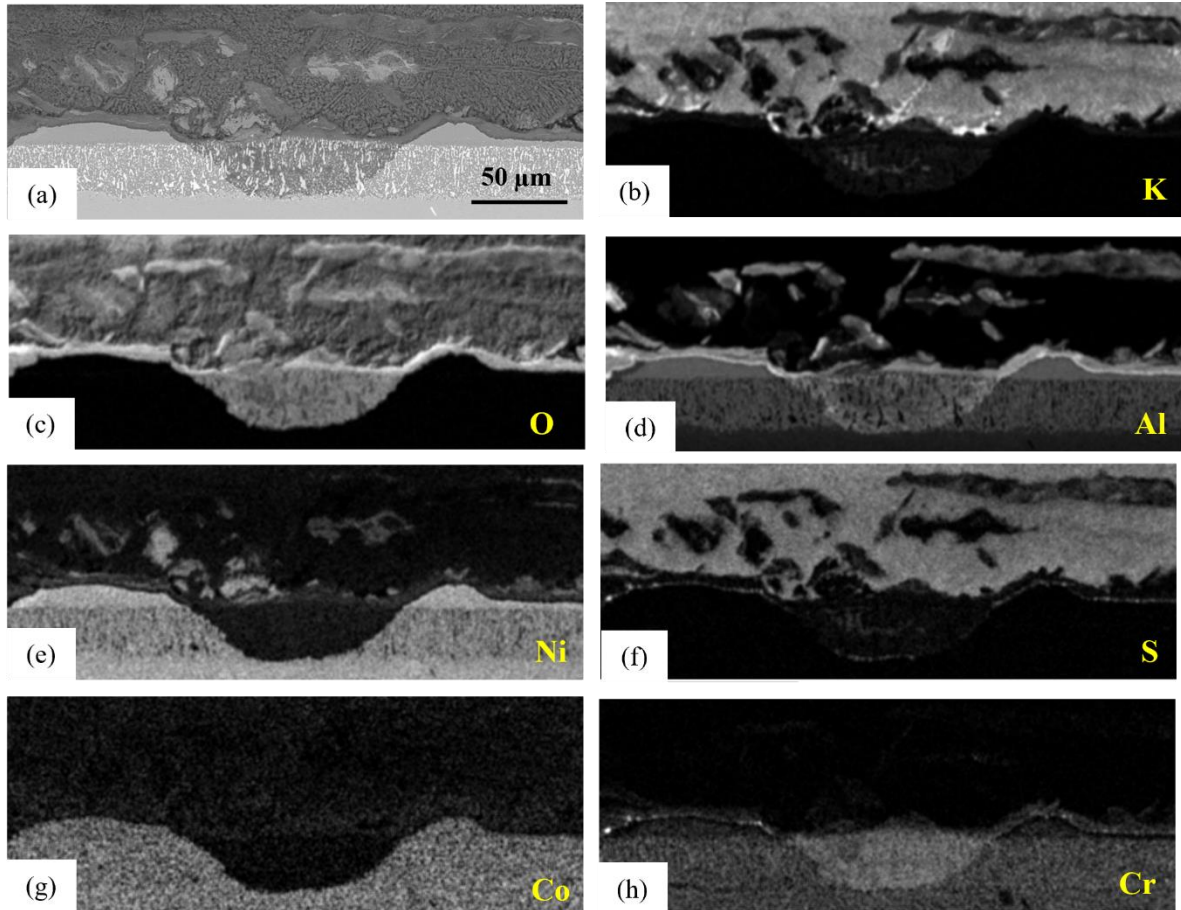


Fig. 10 (a) SEM-BSE image and (b)-(h) corresponding EDX-elemental maps of cross-section of studied β -NiAl coating on Ni-base superalloy after hot-corrosion testing with K_2SO_4 at 700 °C in air-300 ppm SO_2 for 100 h

With Na_2SO_4 -20 K_2SO_4 as the deposit, a porous Al-rich oxide layer was also found as the main morphology characteristics, as shown in Fig. 11. But different from the morphology with Na_2SO_4 , with Na_2SO_4 -20 K_2SO_4 the Al-rich oxide layer was thicker. The Al-rich oxides were intermixed with Ni oxide/sulphide bands, indicating a more severe attack with the binary deposit compared to unary Na_2SO_4 . In addition, voids can be observed between the Al and Ni-rich corrosion products.

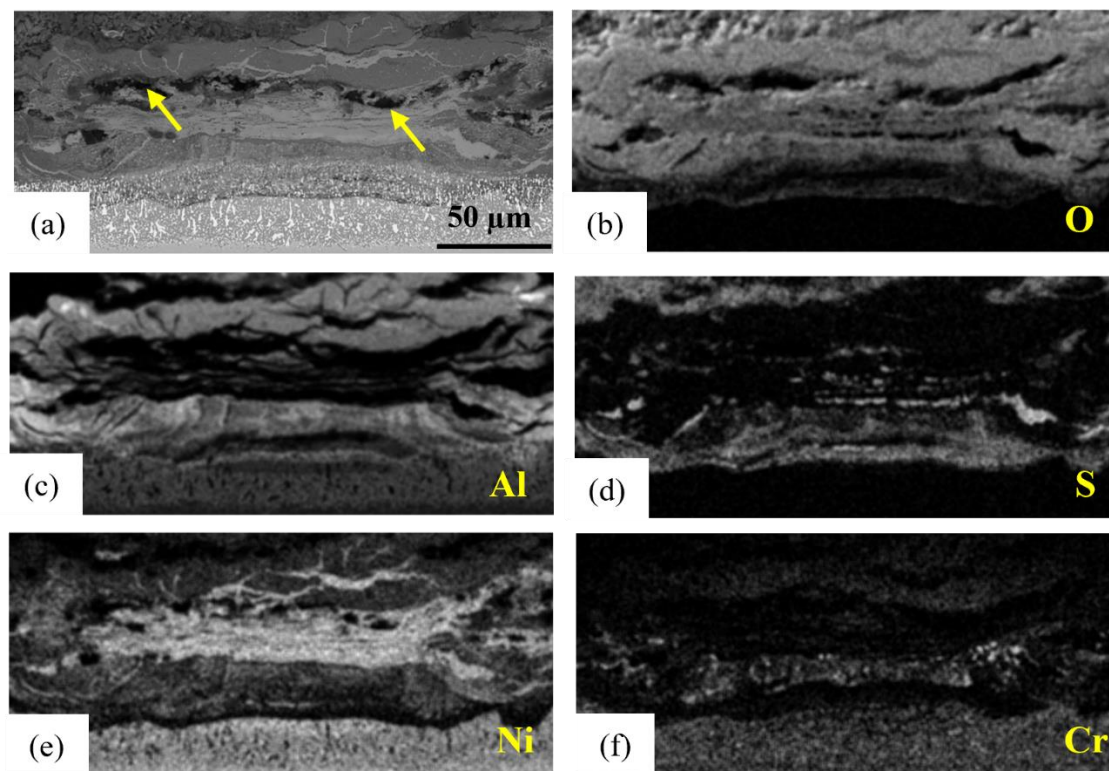


Fig. 11 (a) SEM-BSE image and (b)-(f) corresponding EDX-elemental maps of cross-section of studied β -NiAl coating on Ni-base superalloy after hot-corrosion testing with Na_2SO_4 - $20\text{K}_2\text{SO}_4$ at $700\text{ }^\circ\text{C}$ in air-300 ppm SO_2 for 100 h. The arrows designate the voids.

To better understand the reaction mechanisms between the salt and the coating during the exposure, the salt-rich part of the specimen cross-section with Na_2SO_4 - $20\text{K}_2\text{SO}_4$ deposit was also examined using SEM and EDX, and the corresponding results are shown in Fig. 12 and Table 3. The major reaction products in four different zones in Fig. 12a are marked as A, B, C, and D. Ni and Co distribute homogeneously in zones A, B and C; K is mainly present in zones B and C, but also found in zone A. Na is more enriched in zone D, but also found in the other three zones.

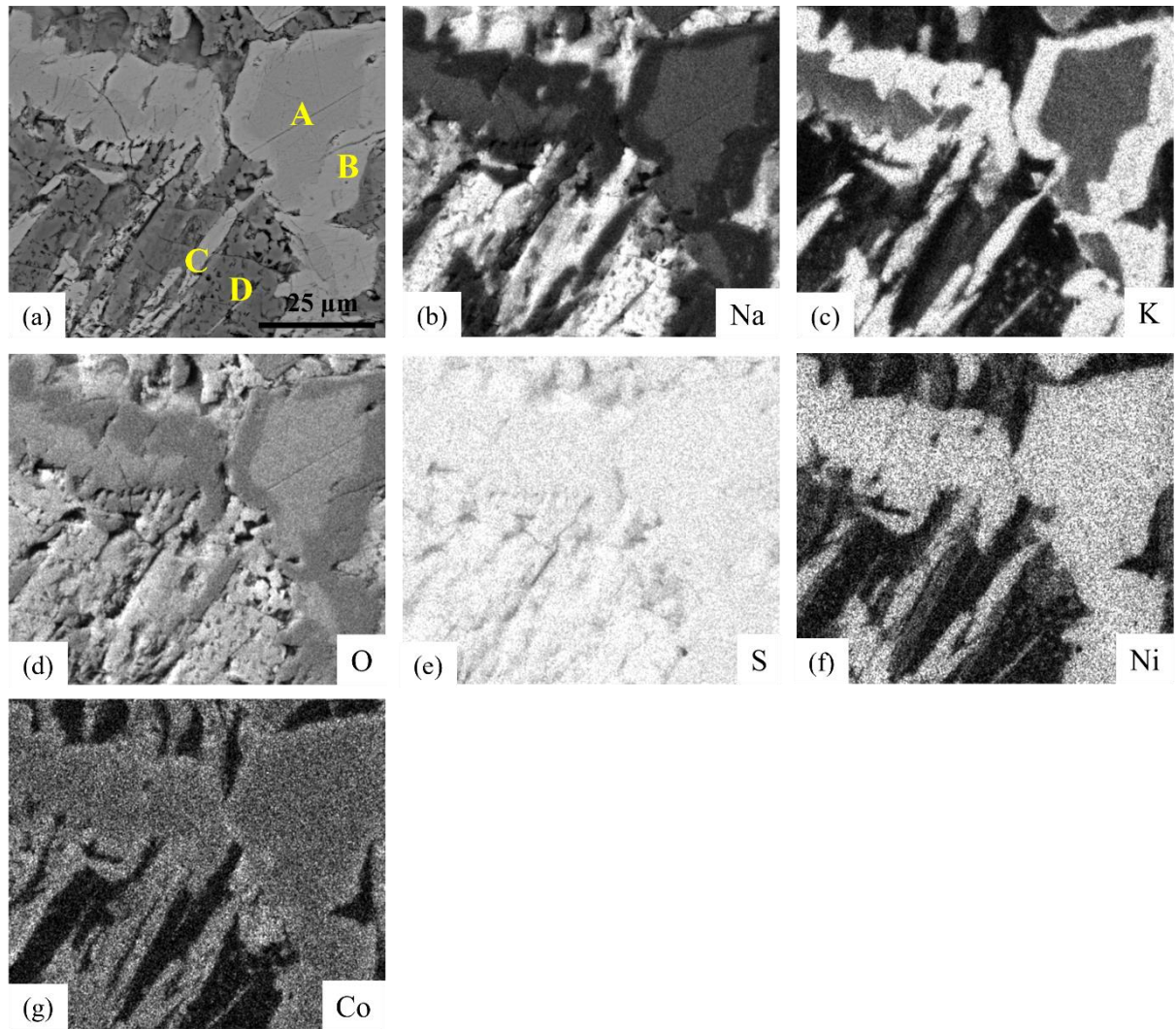


Fig. 12 (a) SEM-BSE image and (b)-(g) corresponding EDX-elemental maps of cross-section of studied β -NiAl coating on Ni-base superalloy after hot-corrosion testing with Na_2SO_4 - $20\text{K}_2\text{SO}_4$ at 700 °C in air-300 ppm SO_2 for 100 h. A-D designate different phases, the composition of which are given in Table 3

Table 3 EDX point analysis of element concentrations of zones A-D in Fig. 12 (at. %)

Spectrum	O	S	Na	K	Ni	Co
A	61.7	15.6	12.6	2.9	5.7	1.6
B	61.4	15.4	7.4	8.4	5.6	1.8
C	61.5	15.5	6.7	9.4	4.5	2.5
D	57.5	14.4	26.8	0.9	0.4	0.0

3.3 The reactions between alkali salts and NiO/NiSO₄ powders

The results of the hot corrosion tests in Section 3.1-3.2 indicate that the reactions involving the sulphate salts and NiO are essential for the hot corrosion reactions. However, clarification of the corrosion mechanisms based on the analysis of corrosion products of the aluminised specimens is difficult due to the presence of Al as well as other alloying elements such as Co and Cr in the coating. In addition, access of the gas phase to the specimen surface can be locally different causing variation in the extent of the attack. To better understand the reaction mechanisms, five powder mixtures consisting of alkali salts and NiO or NiSO₄ were prepared. The compositions are listed in Table 4. 38 mol.% NiO and/or NiSO₄ was added into the alkali salts because it corresponds to the NiSO₄ content in the Na₂SO₄-NiSO₄ eutectic system [22]. The powder mixtures were exposed directly to air + 300 ppm SO₂ for 24/100 h by being placed in open alumina crucibles and subsequently analysed by SEM-EDX and XRD. The BSE images of cross-sections and the corresponding EDX-maps of the powders are presented in Fig. 13-Fig. 15. For the Na₂SO₄-38 mol.% NiO mixture after 100 h exposure, apart from Na₂SO₄ (dark particles) and NiO (bright particles), no third phase was found (Fig. 13). The EDX point analysis (Fig. 13, Table 5) showed that about 1.7 at.% Ni dissolved into Na₂SO₄.

Table 4 The composition of the alkali salt and NiO/NiSO₄ powder mixtures

Mixture	Composition (mol. %)
1	Na ₂ SO ₄ -38NiO
2	K ₂ SO ₄ -38NiO
3	Na ₂ SO ₄ -20K ₂ SO ₄
4	Na ₂ SO ₄ -12.4K ₂ SO ₄ -38NiO
5	Na ₂ SO ₄ -12.4K ₂ SO ₄ -38NiSO ₄

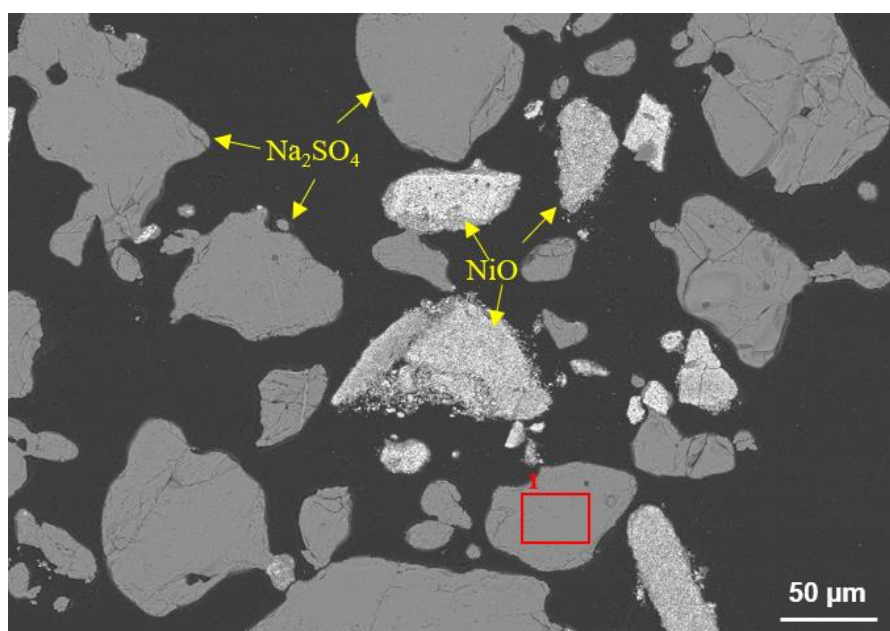


Fig. 13 SEM-BSE image of cross-section of Na₂SO₄-38NiO mixture after exposure at 700 °C in air-300 ppm SO₂ for 100 h. The composition of the area marked by the red box is given in Table 5

Table 5 EDX point analysis of element concentrations of the Na₂SO₄ particle in Fig. 13 (at. %)

Spectrum	O	S	Na	Ni
1	57.8	14.4	26.2	1.7

Different from Na_2SO_4 , K_2SO_4 reacted with NiO to form a lamellar microstructure already after 24 h exposure, as proved by the EDX-maps shown in Fig. 14. The morphology is qualitatively similar to that of the outer part of the reaction product of the NiAl coating after exposure with K_2SO_4 (Fig. 9). No Ni was found in the K_2SO_4 particles by EDX analysis.

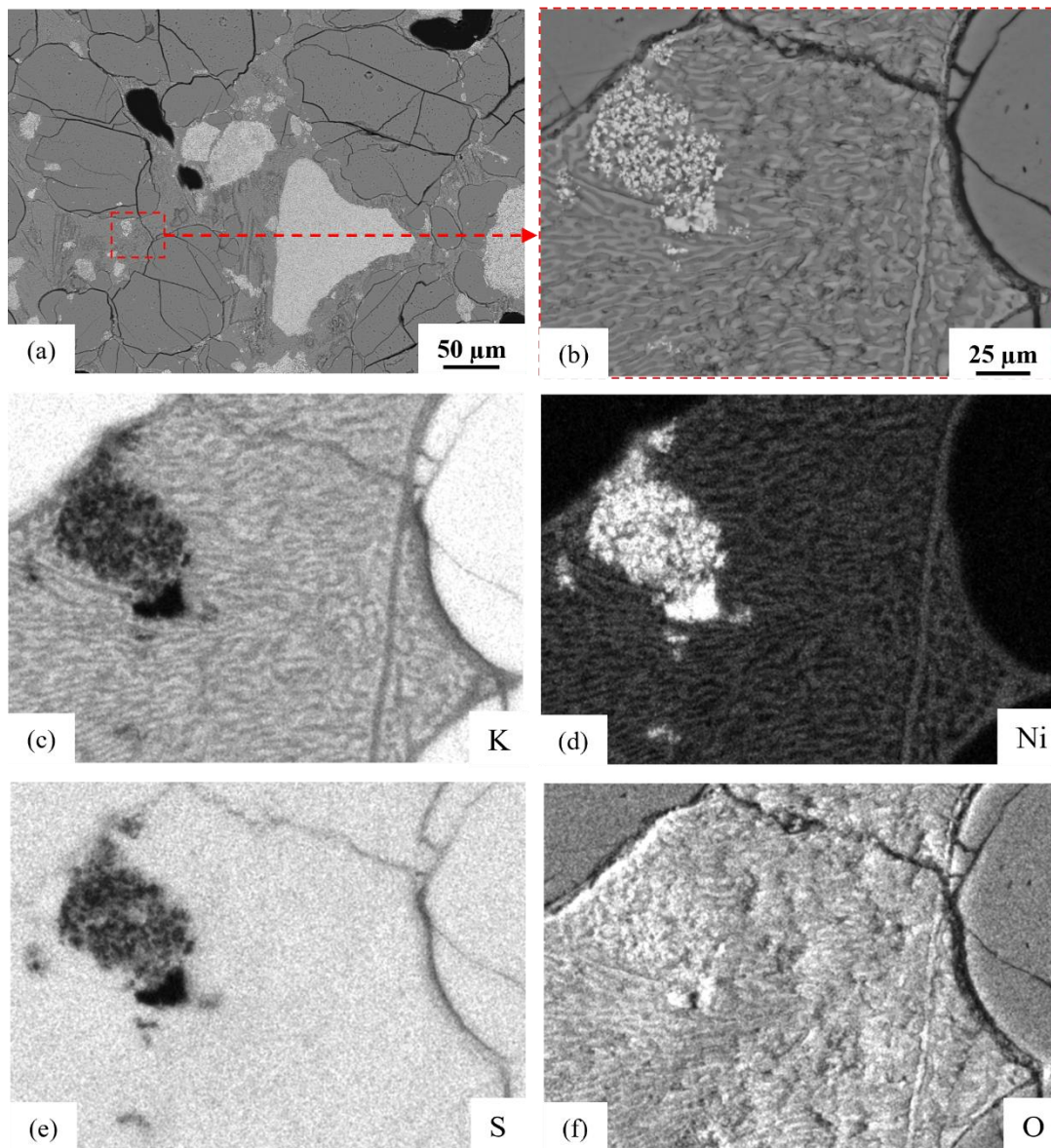


Fig. 14 (a)-(b) SEM-BSE images (b is a higher magnification of the area marked by the red box in a with rotation) and (c)-(f) corresponding EDX-elemental maps of cross-section of K_2SO_4 -38NiO mixture after exposure at 700 °C in air-300 ppm SO_2 for 24 h

Fig. 15a and b show the cross-section image of the Na_2SO_4 -20 K_2SO_4 mixture after 24 h exposure at 700 °C. The microstructure and the EDX analysis (Table 6) reveal that apart from Na_2SO_4 phase, a Na, K sulphate solid solution phase (spectrum 1 in Fig. 15b and Table 6) was present in the mixture. With addition of 38% NiO into the Na_2SO_4 -20 K_2SO_4 mixture (the composition is Na_2SO_4 -12.4 K_2SO_4 -38NiO) and after 100 h exposure, the Na, K sulphate solid solution phase (Fig. 15a-b) disappeared, and a new needle-like phase was observed throughout the Na_2SO_4 solution (spectrum 3 in Fig. 15d). The composition of the needle-like phase shown in Fig. 15d is given in Table 6. The Na_2SO_4 -12.4 K_2SO_4 -38NiO mixture after 24 h exposure exhibits essentially the same microstructure as that after 100 h exposure.

Different from the particle morphologies observed in the Na_2SO_4 -38NiO (Fig. 13), Na_2SO_4 -20 K_2SO_4 (Fig. 15a and b) and Na_2SO_4 -12.4 K_2SO_4 -38NiO (Fig. 15c and d) mixtures, no dispersed particles can be seen in the microstructure of the Na_2SO_4 -12.4 K_2SO_4 -38NiO mixture (Fig. 15e and f), indicating its complete melting during 24 h exposure. This agrees well with the differential thermal analysis (DTA) showing that this mixture starts to melt at 596 °C (Fig. S1 in the supplementary 1). Apart from the dark Na_2SO_4 and the needle-like phase, another phase was observed (spectrum 6) as shown in Fig. 15e - f and the brightness of the latter phase is in between that of the

dark Na_2SO_4 and the bright needle-like phase. The compositions of all three phases are shown in Table 6 (spectra 5-7).

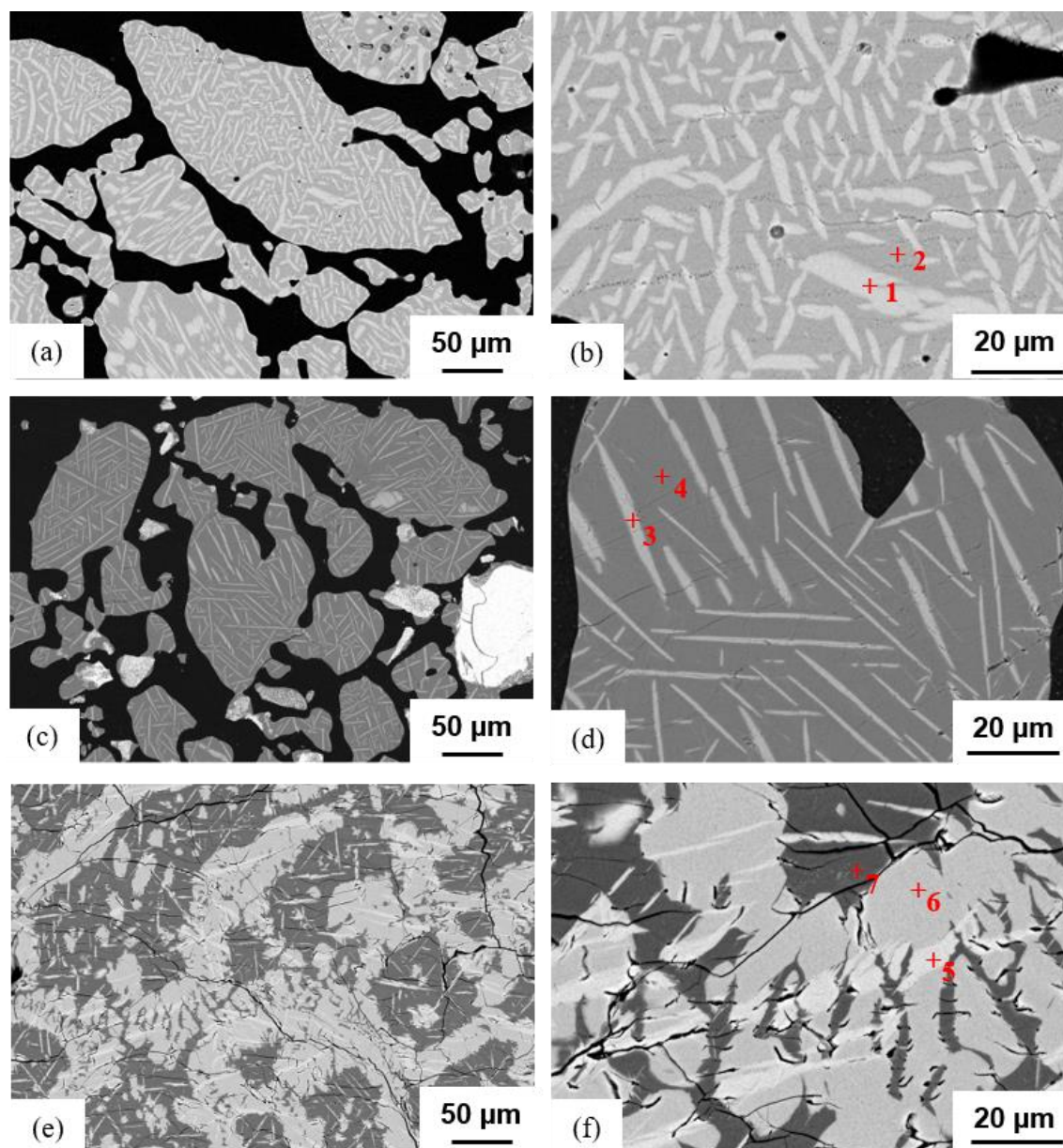


Fig. 15 SEM-BSE image of cross-sections of (a) (b) Na_2SO_4 - $20\text{K}_2\text{SO}_4$ mixture after exposure at $700\text{ }^\circ\text{C}$ in air-300 ppm SO_2 for 24 h; (c) (d) Na_2SO_4 - $12.4\text{K}_2\text{SO}_4$ - 38NiO mixture after exposure at $700\text{ }^\circ\text{C}$ in air-300 ppm SO_2 for 100 h; (e) (f) Na_2SO_4 - $12.4\text{K}_2\text{SO}_4$ - 38NiSO_4 mixture after exposure at $700\text{ }^\circ\text{C}$ in air-300 ppm SO_2 for 24 h. Points designated 1-7 indicate locations of EDX point analyses and the corresponding results are summarized in Table 6.

Table 6 Elemental concentrations (at. %) of locations in Fig. 15 determined by EDX point analysis

Powder mixture	Spectrum	O	S	Na	K	Ni
Na₂SO₄-20K₂SO₄	1	57.6	14.6	17.0	10.8	-
	2	57.8	14.7	25.3	2.2	-
Na₂SO₄-12.4K₂SO₄-38NiO	3	63.0	16.6	7.3	7.2	5.9
	4	57.6	14.4	25.3	1.9	0.8
Na₂SO₄-12.4K₂SO₄-38NiSO₄	5	61.7	15.6	6.3	8.8	7.7
	6	61.9	15.6	11.7	3.2	7.7
	7	58.5	14.9	23.9	1.6	1.2

XRD measurements were performed with all three studied mixtures after the 700 °C exposure to correlate the chemical compositions of the reaction products with their crystal structures. For the Na₂SO₄-20K₂SO₄ mixture (pattern (a) in Fig. 16), low temperature (LT) and medium temperature (MT) modifications of Na₂SO₄, as well as the K₃Na(SO₄)₂ phase were identified. It should be noted that the peaks marked as Na₂SO₄ (LT, MT) are slightly shifted to the left from the ideal Na₂SO₄ pattern, which may be related to the dissolution of K₂SO₄ in Na₂SO₄.

For the mixtures containing NiO/NiSO₄ (patterns b and c in Fig. 16), the high temperature (HT) modification of Na₂SO₄ was identified, instead of the Na₂SO₄ (LT, MT) phase. Although the Na₂SO₄ (HT) phase is a not quenchable phase, it can be stabilized by doping with other elements, e. g. Ni [23]. NiO was identified in both Na₂SO₄-12.4K₂SO₄-38NiO and Na₂SO₄-12.4K₂SO₄-38NiSO₄ mixtures. Na₂Ni(SO₄)₂ was identified only in the mixture with NiSO₄, and it most likely is the light grey phase in Fig. 15f with the composition corresponding to spectrum 6 in Table 6. In the mixtures with NiO and with NiSO₄, there are some un-identified peaks. By comparing patterns b and c in Fig. 16, some identical reflections (designated as “unknown phase”) can be found, e. g. the peak near 9.7°, 13.6°, a triplet between 21° and 22.5°, and a triplet between 29° and 30.5°, indicating the same unknown phase but with slightly different lattice parameters. It is highly likely that this unknown phase is the needle-like phase in Fig. 15c-f, which could be a Na, K, Ni ternary sulphate with cation ratio close to 1:1:1 according to the EDX quantification (compare spectra 3 and 5 in Table 6). Unfortunately, there are no matching entries with this unknown phase in the powder diffraction database (PDF-2 [20]) or in the inorganic Crystal Structure Database (ICSD, [19]). Further studies are thus required to determine the exact crystallographic structure of this ternary phase.

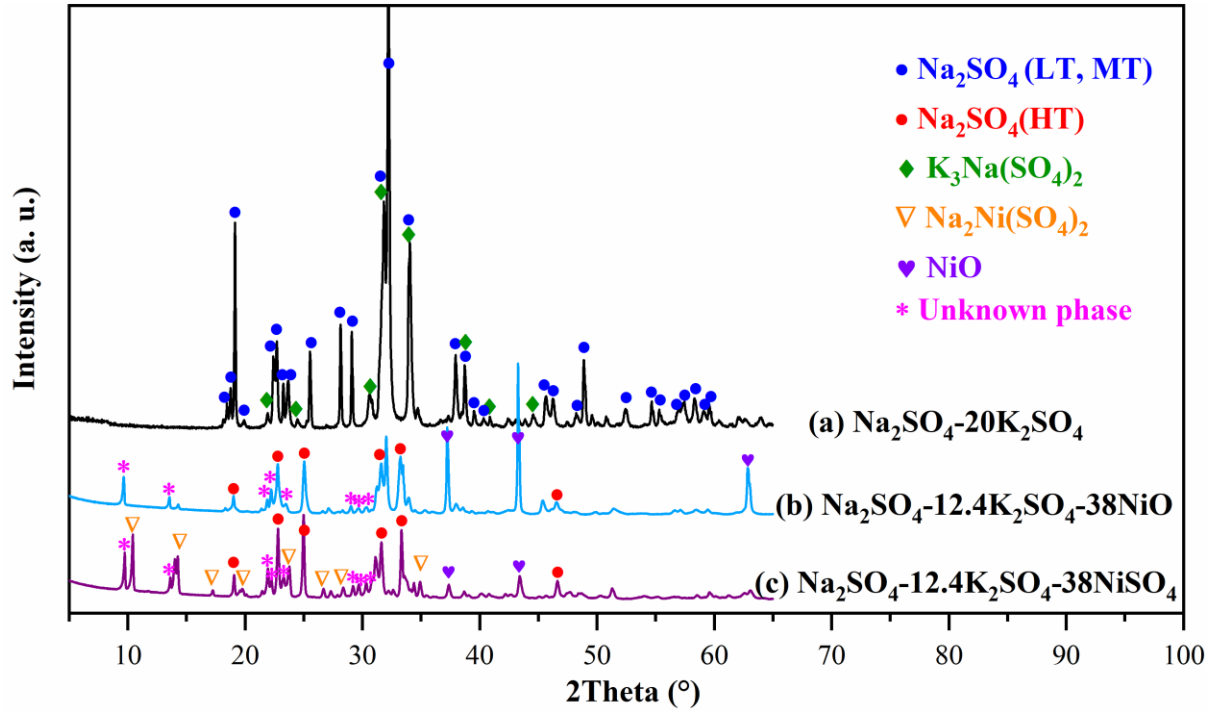


Fig. 16 X-ray patterns of fine powder mixtures consisting of: (a) $\text{Na}_2\text{SO}_4\text{-}20\text{K}_2\text{SO}_4$; (b) $\text{Na}_2\text{SO}_4\text{-}12.4\text{K}_2\text{SO}_4\text{-}38\text{NiO}$; (c) $\text{Na}_2\text{SO}_4\text{-}12.4\text{K}_2\text{SO}_4\text{-}38\text{NiSO}_4$ after exposure at 700 °C in air-300 ppm SO_2 for 24 h; Na_2SO_4 LT, MT and HT in the legend represent the low temperature (LT), medium temperature (MT) and high temperature (HT) Na_2SO_4 modifications, respectively.

4. Thermodynamics of the $\text{Na}_2\text{SO}_4\text{-K}_2\text{SO}_4\text{-NiO-SO}_3$ system

4.1 General remarks

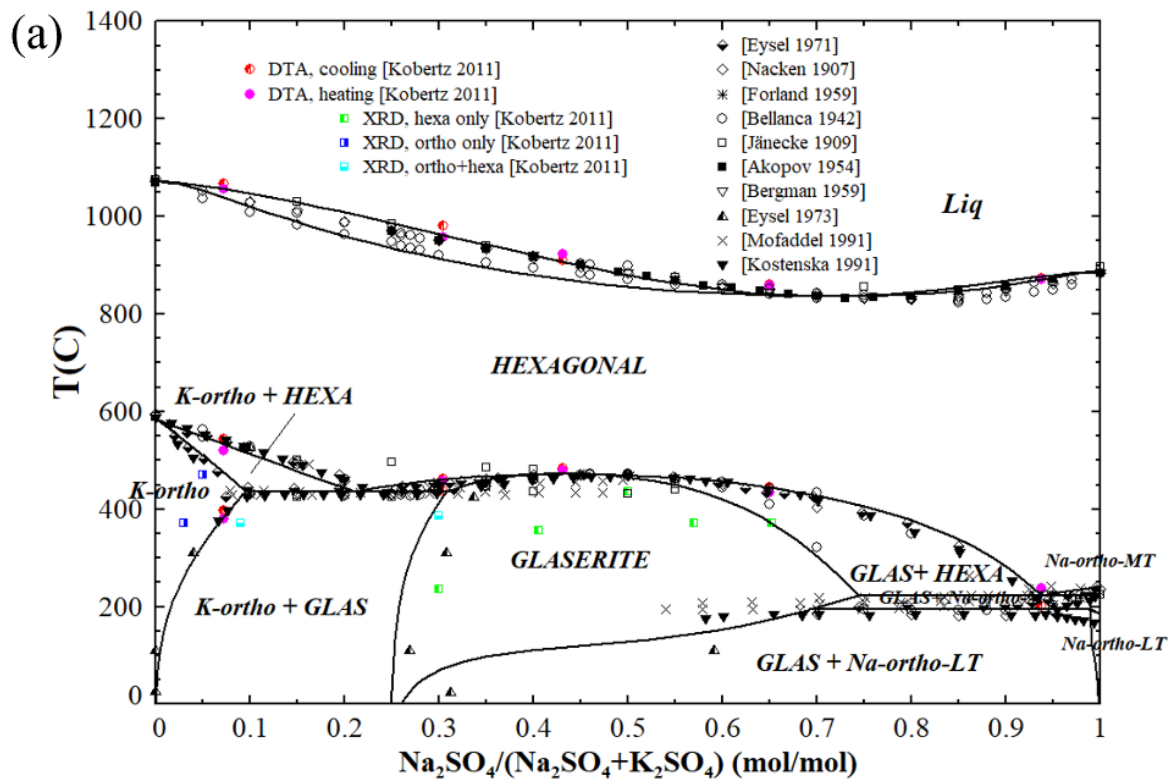
In order to interpret the experimental results obtained in the previous section and derive mechanisms of the corrosion reactions, an extensive assessment of the available thermodynamic data in the investigated system $\text{Na}_2\text{SO}_4\text{-K}_2\text{SO}_4\text{-NiO-SO}_3$ was performed. To predict the conditions for liquid formation considering temperature, SO_3 partial pressure and deposit composition, a reliable thermodynamic database containing all relevant species is required. Specifically, for $\text{Na}_2\text{SO}_4\text{-K}_2\text{SO}_4$ induced hot corrosion

of a Ni-based alloy or coating, the thermodynamic data for the $\text{Na}_2\text{SO}_4\text{-K}_2\text{SO}_4\text{-NiSO}_4$ system is the basis. A sulphate database (GTOX) including the $\text{Na}_2\text{SO}_4\text{-K}_2\text{SO}_4$ system was previously developed by Yazhenskikh et al. [24]. The thermodynamic description of the $\text{K}_2\text{SO}_4\text{-NiSO}_4$ system was presented in our recent work [25]. The $\text{Na}_2\text{SO}_4\text{-NiSO}_4$ phase diagram was reported in 1956 [22]. NiSO_4 was implemented into the GTOX database based on all available data of the $\text{Na}_2\text{SO}_4\text{-K}_2\text{SO}_4\text{-NiSO}_4$ system [22, 25, 26]. The extended database was employed in the current calculations, which were performed using FactSage 7.3 [27].

4.2 Quasi-binary phase diagrams of the $\text{Na}_2\text{SO}_4\text{-K}_2\text{SO}_4\text{-NiSO}_4$ system

The quasi-binary phase diagrams of the $\text{Na}_2\text{SO}_4\text{-K}_2\text{SO}_4$, $\text{Na}_2\text{SO}_4\text{-NiSO}_4$ and $\text{K}_2\text{SO}_4\text{-NiSO}_4$ system were reported in the literature (Fig. 17) [22, 24, 25, 28]. The minimum melting temperature in the $\text{Na}_2\text{SO}_4\text{-K}_2\text{SO}_4$ system is reported by Bellanca et al. [29] to be 830 °C with the composition of $\text{Na}_2\text{SO}_4\text{-20 mol.}\%$ K_2SO_4 . There is a solid solution hexagonal phase (HEXA), which forms based on the high temperature modification of the alkali sulphates with the hexagonal structure. No intermediate compounds were found in this system (Fig. 17a). The minimum melting temperature in the $\text{Na}_2\text{SO}_4\text{-NiSO}_4$ system was reported by Bol'shakov and Fedorov [22] to correspond to the eutectic reaction (671 °C). The hexagonal solid solution phase also exists in the $\text{Na}_2\text{SO}_4\text{-NiSO}_4$ system, and the maximum solubility of NiSO_4 in the hexagonal phase is around 30 mol.% (Fig. 17b). An intermediate compound $\text{Na}_2\text{Ni}(\text{SO}_4)_2$ (congruent melting temperature: approximately 700 °C [22]) prevails in this system (Fig. 17b). In the $\text{K}_2\text{SO}_4\text{-NiSO}_4$ system, there are two eutectics with respective melting temperatures

of 812 °C and 642 °C. An extremely low mutual solubility of the sulphates in the solid state and formation of an intermediate compound $K_2Ni_2(SO_4)_3$ with a melting temperature of 834 °C can be noted. Based on all published data, a database containing all three quasi-binary sub-systems of the Na_2SO_4 - K_2SO_4 - $NiSO_4$ system was developed in-house [24, 25, 28] and was used for the calculations of stability diagrams in the following section.



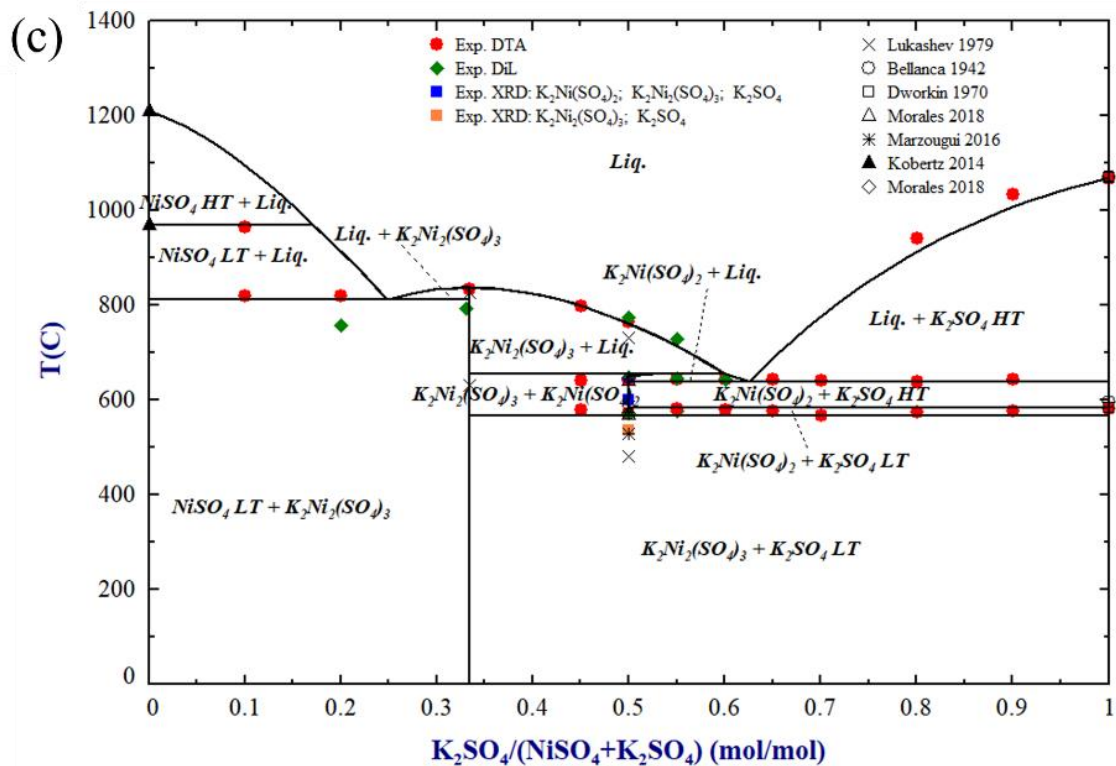
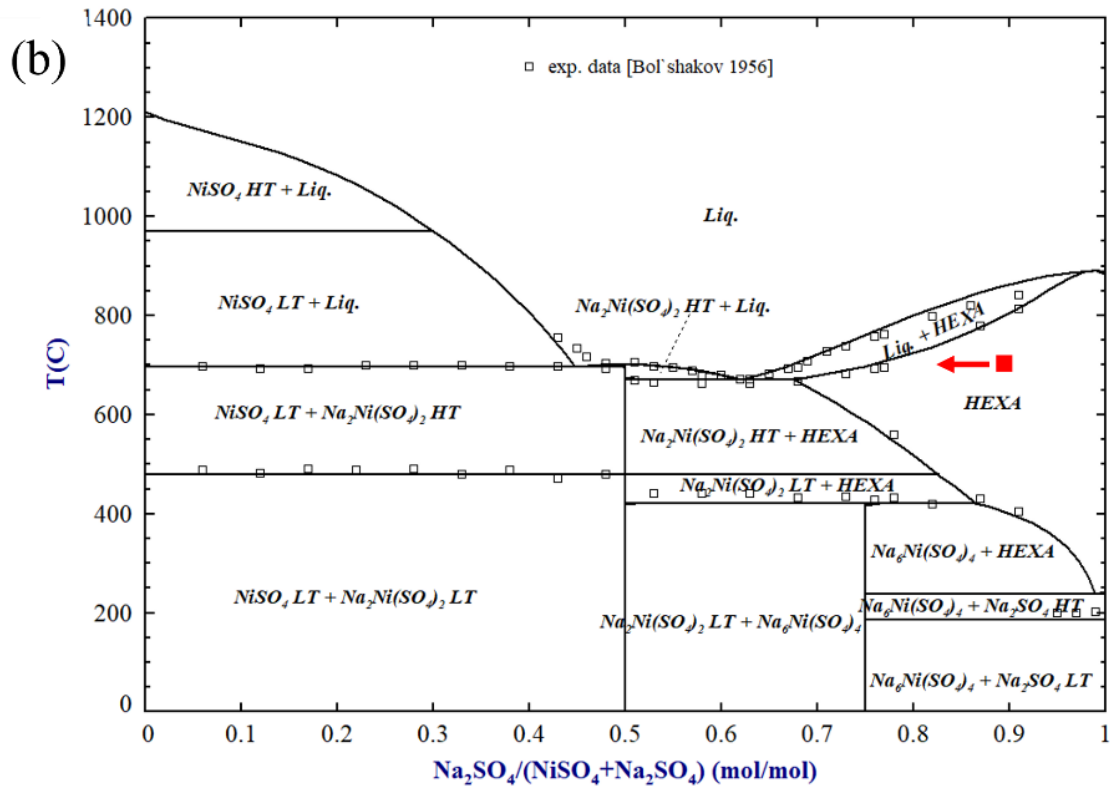


Fig. 17 The calculated phase diagrams with experimental data of (a) $\text{Na}_2\text{SO}_4\text{-K}_2\text{SO}_4$ system [24]; (b) $\text{Na}_2\text{SO}_4\text{-NiSO}_4$ system [28]; (c) $\text{K}_2\text{SO}_4\text{-NiSO}_4$ system [25]. HEXAGONAL (HEXA)

and GLASERITE (GLAS) represent solid solution phases based on Na and K sulphates. K-ortho, Na-ortho-MT and Na-ortho-LT are solution phases with orthorhombic structure based on K_2SO_4 (low temperature modification), Na_2SO_4 (medium and low temperature modifications), respectively. Red symbol and arrow in (b) represent a special composition and the changing direction of this composition with increasing of $NiSO_4$ content at 700 °C, respectively, and will be referred to in the discussion section.

4.3 Stability diagrams of the Na_2SO_4 - K_2SO_4 - NiO - SO_3 system

Phase equilibria in the Na_2SO_4 - K_2SO_4 - NiO - SO_3 system as function of SO_3 partial pressure and temperature were calculated. For the calculations, O_2 , SO_2 , SO_3 , and inert gas (Ar) were chosen as gas constituents. The total gas pressure and the partial pressure of O_2 were set at 1 atm. and 0.21 atm., respectively. The SO_3 partial pressure was varied from 10^{-7} to 0.1 atm. and the temperature from 600 °C to 900 °C. For the corresponding calculations, $0.62 Na_2SO_4 + 0.38 NiO$, $0.62 K_2SO_4 + 0.38 NiO$, and $0.496 Na_2SO_4 + 0.124 K_2SO_4 + 0.38 NiO$, were defined as the compositions of the condensed phases based on the minimum melting temperatures in the corresponding quasi-binary systems showed by the phase diagrams (Fig. 17).

The calculated stability diagrams representing the phase equilibria are provided in Fig. 18, where Fig. 18a, b, and c are present for the Na_2SO_4 - NiO - SO_3 , K_2SO_4 - NiO - SO_3 , and Na_2SO_4 - K_2SO_4 - NiO - SO_3 systems, respectively. The phases involved are liquid phase, NiO , intermediate sulphate compound phases (Na-Ni and K-Ni), and the solid solution phases (HEXA) containing Na, K, Ni sulphate [24, 25, 28].

Since the presence of molten deposit is the pre-requisite for the initiation of rapidly progressing hot corrosion, the emphasis of this assessment is placed on predicting the temperature and gas composition, which favour the formation of the liquid phases. In terms of temperature, in the $\text{Na}_2\text{SO}_4\text{-NiO-SO}_3$ system, the lowest temperature, at which the liquid phase can be expected, is calculated to be $670\text{ }^\circ\text{C}$, as marked by the pink point in Fig. 18a; while in the $\text{K}_2\text{SO}_4\text{-NiO-SO}_3$ and the $\text{Na}_2\text{SO}_4\text{-K}_2\text{SO}_4\text{-NiO-SO}_3$ systems, this temperature was predicted to be $640\text{ }^\circ\text{C}$ (Fig. 18b) and $596\text{ }^\circ\text{C}$ (Fig. 18c), respectively. It is thereby concluded that compared to Na_2SO_4 , K_2SO_4 produces liquid at a lower temperature if the NiO and SO_3 contents in the system are sufficiently high.

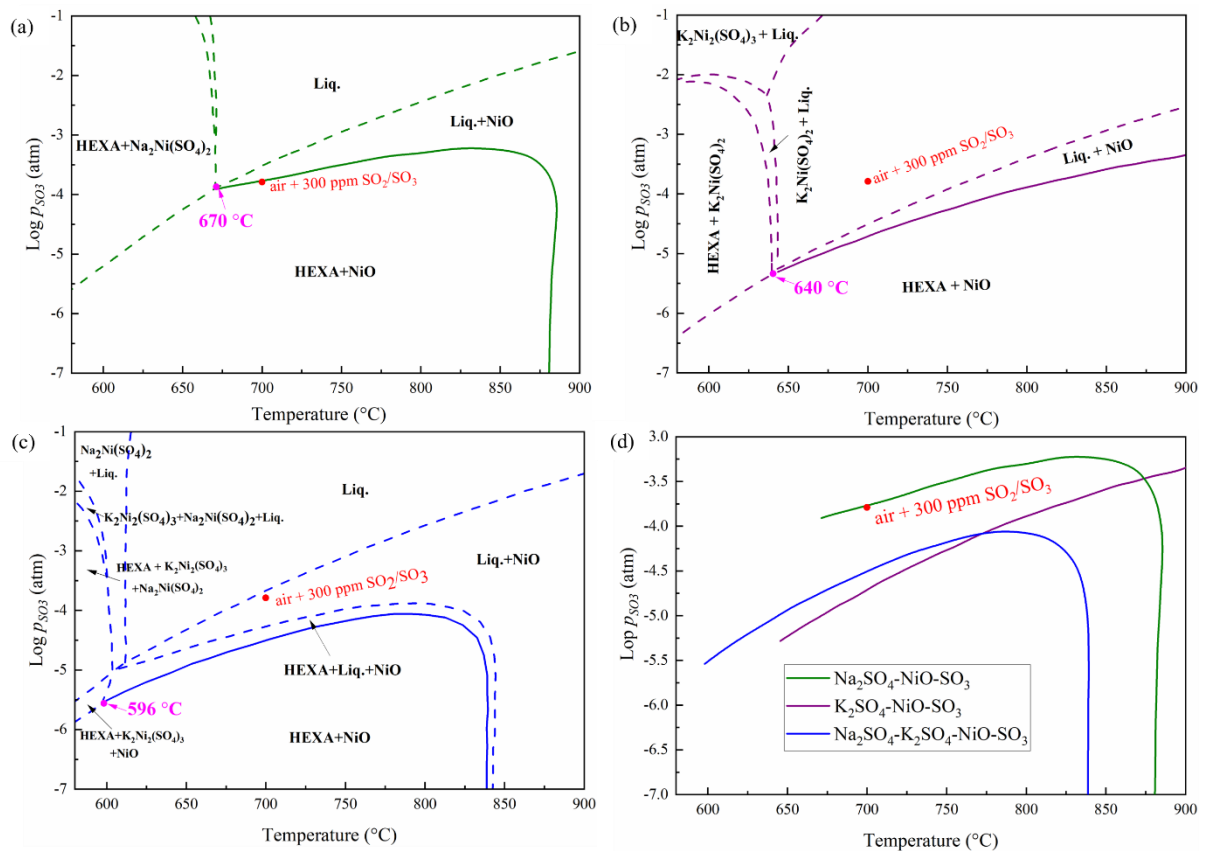


Fig. 18 The calculated stability diagrams: a) Na₂SO₄-NiO-SO₃; b) K₂SO₄-NiO-SO₃; c) Na₂SO₄-K₂SO₄-NiO-SO₃ (compositions of the various base mixtures given in the text); at fixed $p_{O_2} = 0.21$ atm. d) Comparison of the ‘solidus’ line of the three studied systems. HEXA represents a solid solution phase (see Fig. 17) based on the high-temperature modifications of Na and K sulphates. The settings of the calculation are given in the text.

Apart from temperature, the calculated diagrams in Fig. 18 also provide an insight into the influence of p_{SO_3} on the phase equilibria. The bottom solid lines in the diagrams in Fig. 18a, b and c represent the minimum p_{SO_3} required for liquid phase formation as a function of temperature, which are called ‘solidus’ lines in the following text. Fig. 18d summarizes the ‘solidus’ lines in the three calculated systems for comparison. It can be seen that lower p_{SO_3} is required with K₂SO₄ compared to Na₂SO₄ to form liquid phase by reaction with NiO in the temperature range between around 670 °C and 830 °C. The corresponding minimum p_{SO_3} for the binary alkali sulphate is lower than that for pure Na₂SO₄ but higher than that for pure K₂SO₄. The equilibrium SO₃ partial pressure in the presently performed hot corrosion experiments, i.e. air + 300 ppm SO₂/SO₃ at 700 °C was calculated to be 160 ppm ($\log(p_{SO_3}) = -3.79$ atm). This point ($\log(p_{SO_3}) = -3.79$ atm, T = 700 °C) is extremely near but slightly below the ‘solidus’ line in the Na₂SO₄-NiO-SO₃ system, as marked by the red point in Fig. 18a. The activities of the HEXA, NiO, and liquid phase at this point are 1, 1, and 0.997, respectively, indicating the instability of the liquid phase (see the exact phase equilibria in the supplementary 2). The same point is in the liquid region in the K₂SO₄-NiO-SO₃ system, and in the solid + liquid region in the Na₂SO₄-K₂SO₄-NiO-SO₃ system (red

point in Fig. 18b and c). Thus, liquid formation is predicted to occur in the presently used experimental condition under both K_2SO_4 containing deposits but hardly with solely Na_2SO_4 deposit.

5. Discussion

5.1 Na_2SO_4 induced hot corrosion

The 24 h and 100 h exposure at 700 °C of the NiAl coating with pure Na_2SO_4 in air + 300 ppm SO_2 resulted in pitting type (Fig. 1b) and homogeneous type of attack (Fig. 7a), respectively. It is commonly assumed that the type II hot corrosion attack requires formation of molten salt [30-32] due to eutectic reactions, e.g. that in the Na_2SO_4 - $NiSO_4$ system. However, no direct evidence was obtained for molten salt formation during the 100 h exposure of the Na_2SO_4 -38NiO mixture under the present hot corrosion condition. Instead, Ni dissolving into the Na_2SO_4 solid particles was detected (Fig. 13, Table 5). The EDX quantification (Table 5) reveals that the composition of the Na_2SO_4 particles after reacting with NiO is close to a Na_2SO_4 - 11 mol.% $NiSO_4$ mixture. This composition is marked by a red point in the Na_2SO_4 - $NiSO_4$ phase diagram (Fig. 17b). Clearly, this composition corresponds to the Na_2SO_4 solid solution region. In order to produce liquid phase at 700 °C, more than 20 % of $NiSO_4$ is required, as indicated by the red arrow in Fig. 17b.

During exposure of the studied NiAl coating beneath the Na_2SO_4 deposit, $NiSO_4$ was produced by the reaction between NiO, and SO_3 , whereas NiO originates from the oxidation of Ni and/or Ni sulphide. The powder mixture study reveals no indications of

liquid phase formation even with NiO being in contact with Na₂SO₄ (Fig. 13). Therefore, the liquid phase formation process is governed by the SO₃ partial pressure. The calculated stability diagram of the Na₂SO₄-NiO-SO₃ system in Fig. 18a indicates that the p_{SO_3} in the present hot corrosion testing is a bit too low to produce sufficient amounts of NiSO₄ for the liquid phase formation. It is likely to assume that the corrosion attack occurred under the presently used exposure condition (see Fig. 7a) was because of the effect of other alloying elements in the coating or caused by solid state reactions.

It is possible that minor amounts of liquid phase formed between 24 and 100 h exposure due to the presence of alloying elements incorporated into the NiAl-coating from the substrate superalloy during aluminizing process. According to our previous investigation [21], there are 6 at.% Co in the studied coating. The eutectic temperature between Na₂SO₄ and CoSO₄ is 565 °C [22], which is even lower than that of Na₂SO₄-NiSO₄. Thus, the minimum p_{SO_3} required for molten salt formation could be decreased by the presence of Co. In fact, some Co in the corrosion products was observed (Fig. 8g).

Molten salts are considered to be more detrimental compared to the solid ones, because of larger solubility of the oxides as well as the faster transport of e. g. SO₃ in the liquid phase [3, 5]. However, the presence of solid Na₂SO₄ was proved to promote the oxidation and sulfidation of pure Ni at 700 °C even in sulphur free test atmospheres [33, 34]. According to Grégoire et al. [34] Na₂SO₄ releases SO₃ during exposure of pure Ni at 700 °C in dry air for 20 h. Sulphur enrichment was found in the oxide scale at the location where the specimen has no contact with the salt. Moreover, Kistler et. al [35]

proposed recently a mechanism of solid-state hot corrosion reaction induced by Na_2SO_4 at temperatures below the eutectic temperature in the Na_2SO_4 - NiSO_4 system. This mechanism involves formation of a metastable phase $\text{Na}_2\text{Ni}_2\text{SO}_5$ at the grain boundaries of solid Na_2SO_4 , which promotes the outward Ni transport through the deposit. Therefore, it is possible that in the present work the coating under the Na_2SO_4 deposit was in the solid-state hot corrosion regime up to 100 h exposure at 700 °C.

5.2 K_2SO_4 induced hot corrosion

A frontal attack was observed after 24 h and 100 h exposure of the NiAl coating in air + 300 ppm SO_2 with K_2SO_4 (Fig. 1c, Fig. 7d). The reaction between K_2SO_4 and the NiAl coating during 100 h exposure resulted in a lamellar microstructure of the corrosion products, which contain K, Ni, Co, O and S (Fig. 7d, Fig. 9). This morphology was qualitatively reproduced by exposing the K_2SO_4 -38NiO powder mixture to 700 °C in air + 300 ppm SO_2/SO_3 for 24 h (Fig. 14). The powder mixture result confirmed that the lamellar microstructure observed on top of NiAl coating in Fig. 7d was mainly caused by a reaction between K_2SO_4 and Ni from the coating. As shown in Fig. 17c, the solubility of Ni in K_2SO_4 and K in NiSO_4 are nearly zero and there are two intermediate compounds: $\text{K}_2\text{Ni}(\text{SO}_4)_2$ and $\text{K}_2\text{Ni}_2(\text{SO}_4)_3$. The latter compound is stable at lower temperatures. Considering the phase diagram of the K_2SO_4 - NiSO_4 system (Fig. 17c) and the EDX quantification result in Table 2, the lamellar microstructure in Fig. 9 and Fig. 14 is most probably composed of $\text{K}_2\text{Ni}_2(\text{SO}_4)_3$ and K_2SO_4 . The minimum melting temperature of the K_2SO_4 - NiSO_4 system is 642 °C (Fig. 17c, [25]). The calculated stability diagram of the K_2SO_4 -NiO- SO_3 system (Fig. 18b) indicates that a

liquid phase is stable at 700 °C when p_{SO_3} is higher than 19 ppm. Therefore, the p_{SO_3} of 160 ppm in equilibrium condition in air + 300 ppm SO_2/SO_3 is sufficient to stabilize the liquid phase, which agrees very well with the experimental data (Fig. 7d, Fig. 14) showing lamellar microstructures typical for different types of eutectic reactions in metallic and ceramic binary systems [36, 37].

Based on the prevailing results and considerations made by Luthra [5] a mechanism for hot corrosion reaction of K_2SO_4 deposit with the aluminide coating containing minor amount of Cr can be proposed as illustrated with the schematic representation shown in Fig. 19. During the exposure of the studied NiAl coating, NiO and Al rich oxides are produced during transient oxidation (Fig. 19a), especially at 700 °C. NiO further reacts with SO_3 and K_2SO_4 to form a molten salt layer (the yellow area in Fig. 19b). The molten salt layer acts as a barrier layer for the transport of molecular O_2 and SO_2 . In contrast, this layer favours the transport of SO_3 because SO_3 can be transported in the ionic form ($S_2O_7^{2-}$) by reacting with SO_4^{2-} [5]. Effectively SO_3 becomes thus the predominant oxidant at the interface of the salt and the coating (the effective transport of SO_3 is shown by arrows in Fig. 19b). The oxidation of the coating by SO_3 results in formation of Al-rich oxides (Al_2O_3 and spinel, the green region in Fig. 19b) and release of sulphur. Due to very low oxygen activity originating from the presence of molten salt and high sulphur activity, coarse Ni-sulphide precipitates (Fig. 3 and Fig. 19b) and fine internal Cr-sulphide particles ([21] and Fig. 19b) are formed below the Al-rich oxide layer within the coating. Since the eutectic temperature of Ni- Ni_3S_2 is 645 °C [38], i.e. below the test temperature of 700 °C used in the present study,

formation of Ni-sulphide might additionally increase the rate of the corrosion attack, provided that Al was depleted below a critical value. It should be, however, noted that no evidence for liquid phase formation was found associated with the Ni-sulphide particles in the present work.

As the reaction continues, Ni-sulphides are oxidized. NiO dissolves into the molten salt and diffuses outwards in the form of Ni^{2+} (Fig. 19c) and the content of the molten salt thereby increases. The pre-formed Al-rich oxide layer is delaminated from the coating and its pieces become incorporated into the molten deposit (Fig. 9, Fig. 10, and Fig. 19c). The Al-rich oxides do not react in contact with the sulphate melt, supported by the fact that no dissolution of $\text{Al}_2(\text{SO}_4)_3$ into K_2SO_4 was found in the $\text{Al}_2(\text{SO}_4)_3\text{-K}_2\text{SO}_4$ [39] system. Upon cooling, the liquid sulphate solidifies to produce a lamellar structure composed of K_2SO_4 and $\text{Ni}_2\text{K}_2(\text{SO}_4)_3$ and the elongated pieces of Al-rich oxide remain embedded in the deposit (compare EDX-maps in Fig. 9 and schematic in Fig. 19d).

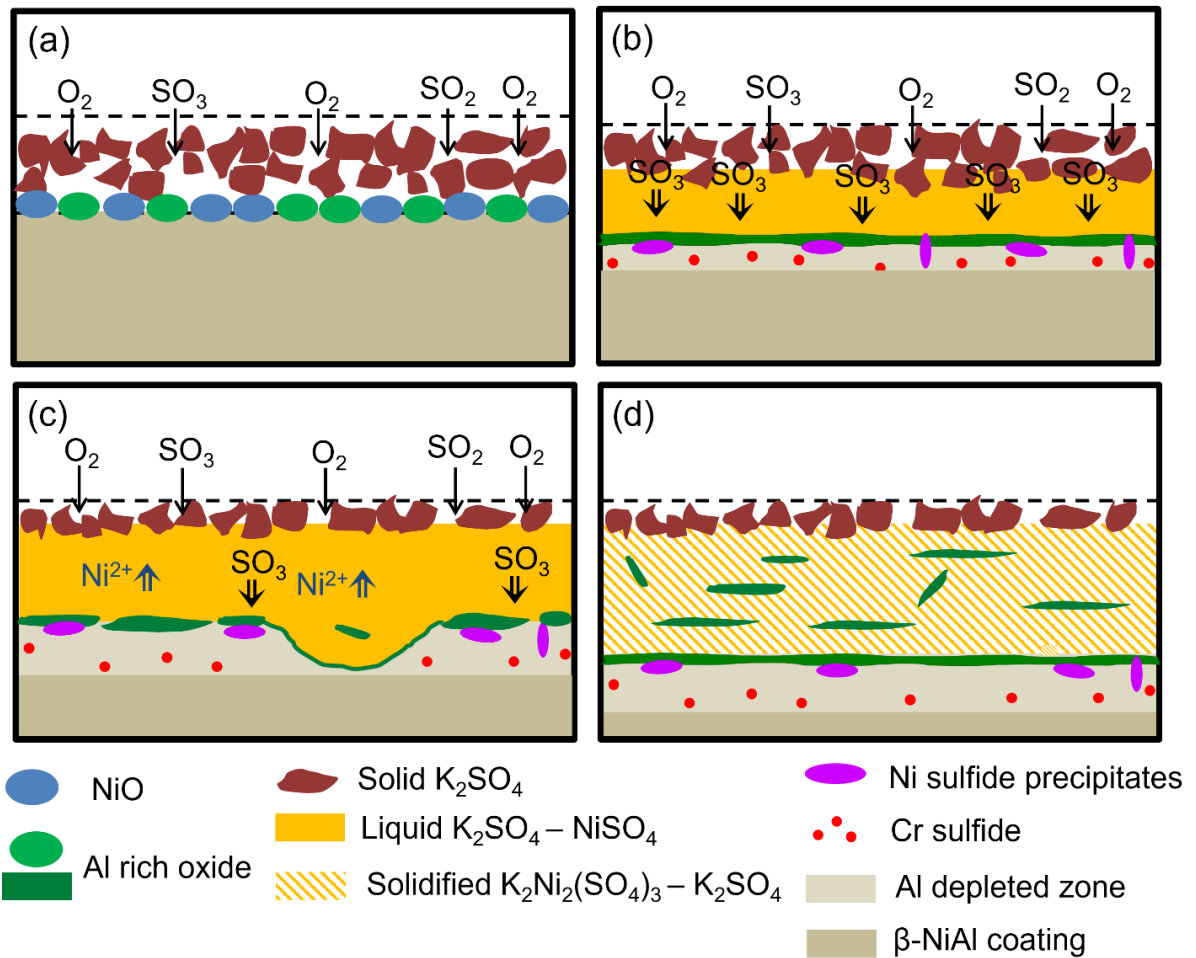


Fig. 19 Schematic representation of microstructural evolution and transport processes during reactions of the studied β -NiAl coating with K_2SO_4 in air + 300 ppm SO_2 at 700 °C: a) initial oxidation of the coating; b) formation of liquid sulphate phase, Al-rich oxides and (internal) Ni and Cr sulphides; c) Ni-transport through the melt and penetration of the melt through the Al-rich oxide layer; d) Al-rich oxide islands formation during longer time exposure and the microstructure of the corrosion products after cooling to room temperature

5.3 Na_2SO_4 -20 K_2SO_4 induced hot corrosion

Severe hot corrosion attack was observed on the NiAl coating with mixed Na_2SO_4 -20 K_2SO_4 deposit after exposure at 700 °C in air + 300 ppm SO_2 for 24 h (Fig.

1d) and especially 100 h (Fig. 7g). Fig. 5 indicates formation of three phases (designated as A, B and C) in the deposit on top of the NiAl-coating after the 24 h test.

By considering the microstructure (Fig. 15a and b), the composition (EDX spectra 1 and 2 in Table 6), the phase identification by XRD (Fig. 16a) of the Na-K mixed sulphate powder, and the associated phase diagram (Fig. 17a, [24]), it is found that the Na_2SO_4 -20 K_2SO_4 mixture is composed of Na_2SO_4 and a glaserite phase after exposure. The glaserite phase is a solid solution phase, which exhibits a variable composition (25 mol.%-75 mol.% Na_2SO_4) formed in the sub-solidus region of the K_2SO_4 - Na_2SO_4 system. The crystal structure of the glaserite phase is based on Na_2SO_4 , whereby part of Na is replaced by K in the cation sublattice [24, 40]. According to the phase diagram in Fig. 17a glaserite is unstable at the test temperature of 700 °C and apparently formed during cooling of the coating (powder specimens) to room temperature. Thus, the dark phase (phase A in Fig. 5) and the bright phase (phase B in Fig. 5) in the salt particles above the NiAl coating are Na_2SO_4 and the glaserite phase, respectively.

The studies of Na_2SO_4 -12.4 K_2SO_4 -38NiO/ NiSO_4 powder mixtures (Fig. 15c-f, spectra 3 and 5 in Table 6, and Fig. 16b-c) indicate that the needle-like phase formed during exposure of the Na_2SO_4 -20 K_2SO_4 mixture on top of the NiAl coating (Fig. 5, phase C marked by the yellow arrows) and in the powder mixtures (Fig. 15d and f) is likely to be a Na, K, Ni ternary sulphate phase with a cation ratio close to 1:1:1. Formation of the needle-like phase might bind K and thereby suppress formation of the glaserite phase, which was found in the salt particles on top of the NiAl coating (phase

B in Fig. 5) but not after the exposure of the $\text{Na}_2\text{SO}_4\text{-}12.4\text{K}_2\text{SO}_4\text{-}38\text{NiO}$ powder mixture (Fig. 15c-d). Another intermediate compound $(\text{Na,K})_2\text{Ni}(\text{SO}_4)_2$ is observed in addition to the Na-K-Ni ternary sulphate in the $\text{Na}_2\text{SO}_4\text{-}12.4\text{K}_2\text{SO}_4\text{-}38\text{NiSO}_4$ powder mixture (spectrum 6 in Fig. 15e-f, Fig. 16c). The absence of $(\text{Na,K})_2\text{Ni}(\text{SO}_4)_2$ in the powder mixture with NiO is most likely related to a relatively slow sulphation of NiO and/or slow incorporation of Ni into Na_2SO_4 (compare with Fig. 13).

The compositions of the reaction products observed in the powder mixtures between Na and K sulphates and NiO/NiSO₄ appeared to be in excellent agreement with the products on the corroded aluminide coatings (compare the EDX-results in Fig. 12, Table 3 and Fig. 15, Table 6, respectively). This agreement indicates that the hot corrosion of the studied coatings is dominated by reactions of Ni with the deposit, and the reactions of Al, Co and Cr probably play a less important role.

Based on the prevailing results of the hot corrosion tests with the aluminide coating and the annealing experiments with the sulphate/oxide powder mixtures, the following chronological sequence can be proposed for the reaction of NiAl with the $\text{Na}_2\text{SO}_4\text{-}20\text{K}_2\text{SO}_4$ deposit. During the early stages of exposure, Ni from the coating is oxidized and Ni-ions diffuse into the solid salt forming a needle-like Na, K, Ni ternary sulphate compound (Fig. 5). Formation of a porous, Al-rich oxide layer (Fig. 1d and Fig. 4) and sulphur accumulation beneath this layer (in the form of Ni-sulphides; compare the morphologies in the left parts in Fig. 4a, e and g after 24 h) are qualitatively similar processes to those described above for the case of K_2SO_4 deposit (Fig. 3 and schematic in Fig. 19). This is an indication that formation of a liquid phase occurred at

least locally beneath the $\text{Na}_2\text{SO}_4\text{-}20\text{K}_2\text{SO}_4$ deposit after relatively short time, supported by the DTA-curve for $\text{Na}_2\text{SO}_4\text{-}12.4\text{K}_2\text{SO}_4\text{-}38\text{NiSO}_4$ mixture shown in the supplementary 1. The Al-oxide layer is not very protective and Ni-sulphide precipitates become eventually exposed to the melt and oxidize, a step followed by oxidation of Al in the underneath coating. The latter process is repeated during further exposure resulting in formation of layered NiO / Al-rich oxide morphology as designated as Zone A in Fig. 4a. With increasing time to 100 h further incorporation of Ni into the deposit results in formation of $(\text{Na,K})_2\text{Ni}(\text{SO}_4)_2$ (compare Fig. 12 / spectrum A in Table 3 and Fig. 15 / spectrum 6 in Table 6; XRD pattern (c) in Fig. 16) and complete deposit melting (the melting temperature of $\text{Na}_2\text{Ni}(\text{SO}_4)_2$ without K is about 700 °C, Fig. 17b). After cooling, both the needle-like Na, K, Ni ternary sulphate compound and $(\text{Na,K})_2\text{Ni}(\text{SO}_4)_2$ were identified on top of the aluminide coating (Fig. 12).

5.4 Comparison of hot corrosion induced by different alkali sulphates

It is generally agreed that molten salts have a greater ability in initiating severe hot corrosion attack, compared to solid and gaseous salts [3-5]. Therefore, when comparing the aggressiveness of the individual alkali sulphates and their mixtures in terms of their ability to induce type II hot corrosion attack, the potential of these three salts for producing liquid is a major aspect. According to our previous work [25], the eutectic temperature of the $\text{K}_2\text{SO}_4\text{-NiSO}_4$ system is 642 °C, which is lower than that of the $\text{Na}_2\text{SO}_4\text{-NiSO}_4$ system (671 °C). The $\text{NiSO}_4\text{-Na}_2\text{SO}_4\text{-K}_2\text{SO}_4$ system might have an even lower eutectic temperature (approximately 596 °C) as shown by the DTA measurements (see supplementary 1). The minimum exposure temperature and p_{SO_3}

required for molten salt formation were found to be lower for the $\text{K}_2\text{SO}_4\text{-NiO-SO}_3$ and the $\text{Na}_2\text{SO}_4\text{-K}_2\text{SO}_4\text{-NiO-SO}_3$ system than that for the $\text{Na}_2\text{SO}_4\text{-NiO-SO}_3$ system (Fig. 18). Lower melting temperature and lower p_{SO_3} required for liquid phase formation with K_2SO_4 are in agreement with the fact that the corrosion attack of the aluminide coating induced by K_2SO_4 and $\text{Na}_2\text{SO}_4\text{-20K}_2\text{SO}_4$ are much more severe than that induced by Na_2SO_4 (Fig. 1 and Fig. 7). A detrimental effect of K_2SO_4 addition to Na_2SO_4 in accelerating hot corrosion attack in Fe-Al and Co-based alloys was reported by Shi et al. [12] and LeBlanc et al. [11], respectively. The associated mechanisms proposed in these studies [11, 12] by considering the experimental observations and thermodynamic assessment are the low eutectic temperature and the low p_{SO_3} required for stabilizing the liquid phase in the K_2SO_4 containing systems, which qualitatively agree with the present work.

In addition to the studies mentioned above [11, 12], thermodynamic considerations regarding liquid phase formation in case of Na_2SO_4 deposit have been extensively studied by Luthra et al. ($\text{Na}_2\text{SO}_4\text{-Co}_3\text{O}_4\text{-SO}_3$ system, [30]) and Misra et al. ($\text{Na}_2\text{SO}_4\text{-NiO-SO}_3$ system, [4]). The trend for liquid phase formation predicted in the present work (Fig. 18a) qualitatively agrees with these studies [4, 30]. However, due to the different model and assumptions applied, the minimum SO_3 partial pressure required for liquid formation ('solidus' line) calculated in the present work is slightly different from that reported by Misra. A detailed comparison with Misra's model was made in our previous work [21]. Moreover, with more precise database and advanced

modelling tool (Factsage), the stability diagram calculation performed in the present work provides more details regarding the phase equilibria, e.g. the ‘liquidus’ line.

Apart from the hot corrosion kinetics, it is also noticed that the products of the reactions between Ni oxide/sulphate and different deposits are different. Referring to the NiSO₄-Na₂SO₄ (Fig. 17b, [28]) and NiSO₄-K₂SO₄ (Fig. 17c, [25]) phase diagrams the solubility of NiSO₄ in Na₂SO₄ hexagonal solid solution is around 30 mol.%; while virtually no dissolution of NiSO₄ in solid K₂SO₄ was found [25]. This means that in the Na₂SO₄-NiSO₄ system a substantial enrichment of Ni in the Na₂SO₄ is required prior to the formation of the liquid phase, which might significantly increase the incubation time prior to liquid-phase-induced hot corrosion reaction. In contrast, no such “buffer” solid solution exists in the K₂SO₄-NiSO₄ system with nearly zero mutual solubility in the solid state. Regarding the Na₂SO₄-20K₂SO₄ deposit case, formation of two compound phases, i.e. the Na, K, Ni ternary sulphate phase with presently unknown structure and the (Na,K)₂Ni(SO₄)₂ phase was detected (Fig. 5, Fig. 12, Fig. 15), whereby the presence of K in the latter phase might additionally stabilize it. Based on the prevailing results it can be hypothesized that formation of the thermodynamically stable mixed sulphate phases might provide an additional driving force for Ni-reaction with the deposit, which effectively increases the corrosion rate. Further studies are required to verify the latter idea.

6. Conclusions

Na_2SO_4 , K_2SO_4 , and $\text{Na}_2\text{SO}_4\text{-}20\text{K}_2\text{SO}_4$ were applied on the surface of a β -NiAl coating on a single-crystal Ni-based superalloy, and then the samples were exposed to 700 °C with air-300 ppm SO_2 for 24 h and 100 h. In addition, a series of alkali salts-NiO/NiSO₄ mixtures were exposed to the same test conditions. The phase stabilities of the $\text{Na}_2\text{SO}_4\text{-K}_2\text{SO}_4\text{-NiO-SO}_3$ system were calculated by FactSage using an in-house developed thermodynamic database. Based on the experimental and calculation results the following conclusions are drawn:

1. For the NiAl coating with Na_2SO_4 local pits were found after 24 h exposure, which developed into an Al-rich mixed oxide/sulphate layer after 100 h exposure. The powder mixture study and the stability diagram calculation did not indicate any liquid phase formation. The attack is likely related to the presence of other alloying elements, e.g. Co or due to solid-state corrosion reactions.
2. During exposure of the NiAl coating with K_2SO_4 , a melt formed according to the observation of the microstructures of the exposed NiAl coating and the powder mixture, as well as the thermodynamic calculation. Consequently, a mixed oxide/salt layer was observed after 24 h exposure; a thick molten salt layer with Al_2O_3 islands was found after 100 h exposure. The solidified salts appeared in the form of $\text{K}_2\text{SO}_4\text{-K}_2\text{Ni}_2(\text{SO}_4)_3$ lamellar mixture indicating a eutectic reaction. The observed rapid corrosion was

promoted by nearly zero solubility of NiSO_4 in K_2SO_4 and a high thermodynamic stability of $\text{K}_2\text{Ni}_2(\text{SO}_4)_3$.

3. The hot corrosion attack caused by the Na_2SO_4 - $20\text{K}_2\text{SO}_4$ binary salt was more severe than that by pure Na_2SO_4 . Mixed Ni, Al rich oxides and Ni sulphide formed during 24 and 100 h exposure. During the early stage of the exposure, a Na, K, Ni sulphate phase with cation ratio of approximately 1:1:1 was produced by the reaction between Ni oxide/sulphate and the Na_2SO_4 - K_2SO_4 solution phase. The crystallography of this ternary sulphate phase does not match any of the known binary compounds in the Na_2SO_4 - NiSO_4 and K_2SO_4 - NiSO_4 systems. After longer time exposure $\text{Na}_2\text{Ni}(\text{SO}_4)_2$ formed and the salt melted. Apparently, addition of K_2SO_4 into Na_2SO_4 lowers the p_{SO_3} required for liquid phase formation. The formation of low-melting liquid and thermodynamically stable Ni, K and Na-containing compounds are believed to accelerate the attack, compared to that caused by the single Na_2SO_4 deposit.

7. Acknowledgements

The authors are grateful to Mr. H. Cosler for performing the hot corrosion tests, to Mr. V. Gutzeit and Mr. J. Bartsch for preparing the cross sections. Dr. E. Wessel and Dr. D. Grüner are kindly acknowledged for the SEM analysis. Mr. M. Ziegner is kindly acknowledged for the XRD analysis. This work was supported by China Scholarship

Council (grant number 201708440229); Federal Ministry of Economic Affairs and Energy and MTU Aero Engines AG (grant numbers: 20T1522A, 20T1302A).

8. Data availability

The raw/processed data required to reproduce these findings can be requested from the corresponding author.

9. Declaration of Competing Interest

The authors declare that they have no known competing financial interests or personal relationships that could have appeared to influence the work reported in this paper.

10. References

- [1] K. J. Meisner and E. J. Opila, Hot corrosion of shipboard gas turbine blades. *Oxidation of Metals*, 2020. 94: 301–322. DOI: 10.1007/s11085-020-09990-7.
- [2] E. Kosieniak, K. Biesiada, J. Kaczorowski, et al., Corrosion failures in gas turbine hot components. *Journal of Failure Analysis and Prevention*, 2012. 12(3): 330-337. DOI: 10.1007/s11668-012-9571-3.
- [3] N. Birks, G. H. Meier, and F. S. Pettit, Introduction to the high-temperature oxidation of metals. 2006: Cambridge university press. 206-252. DOI: 10.1017/CBO9781139163903.
- [4] A. K. Misra, D. P. Whittle, and W. L. Worrell, Thermodynamics of molten sulfate mixtures. *Journal of the Electrochemical Society*, 1982. 129: 1840-1845. DOI: 10.1149/1.2124305.

- [5] K. L. Luthra, Low temperature hot corrosion of cobalt-base alloys: Part II. reaction mechanism. *Metallurgical Transactions A*, 1982. 13A: 1853-1864. DOI: 10.1007/BF02647842.
- [6] R. L. Jones and S. T. Gadomski, Reactions of $\text{SO}_2(\text{SO}_3)$ with $\text{NiO-Na}_2\text{SO}_4$ in nickel-sodium mixed sulfate formation and low temperature hot corrosion. *Journal of the Electrochemical Society*, 1982. 129(7): 1613-1618. DOI: 10.1149/1.2124219.
- [7] G. H. Meier, Invited review paper in commemoration of over 50 years of oxidation of metals: Current aspects of deposit-induced corrosion. *Oxidation of Metals*, 2021. DOI: 10.1007/s11085-020-10015-6.
- [8] F. Pettit, Hot corrosion of metals and alloys. *Oxidation of Metals*, 2011. 76(1-2): 1-21. DOI: 10.1007/s11085-011-9254-6.
- [9] N. S. Bornstein, Reviewing sulfidation corrosion-Yesterday and today. *JOM*, 1996. 48(11): 37-39. DOI: 10.1007/bf03223242.
- [10] D. A. Shifler. The increasing complexity of hot corrosion. in *ASME Turbo Expo : Turbomachinery Technical Conference and Exposition GT*. 2017. DOI: 10.1115/GT2017-65281.
- [11] O. H. LeBlanc, K. L. Luthra, and R. W. Haskell, Thermodynamics of the $\text{Na}_2\text{SO}_4\text{-K}_2\text{SO}_4\text{-CoSO}_4$ system and their relevance to low-temperature hot corrosion. *Oxidation of Metals*, 1989. 31(5): 393-414. DOI: 10.1007/BF00666464.
- [12] L. Shi, Y. Zhang, and S. Shih, The effect of K_2SO_4 additive in Na_2SO_4 deposits on low temperature hot corrosion of iron-aluminum alloys. *Oxidation of Metals*, 1992. 38(5): 385-405. DOI: 10.1007/BF00665661.

- [13] L. Brooking, S. Gray, K. Dawson, et al., Analysis of combined static load and low temperature hot corrosion induced cracking in CMSX-4 at 550 °C. *Corrosion Science*, 2020. 163. DOI: 10.1016/j.corsci.2019.108293.
- [14] L. Brooking, S. Gray, J. Sumner, et al., Interaction of hot corrosion fatigue and load dwell periods on a nickel-base single crystal superalloy. *International Journal of Fatigue*, 2018. 117: 13-20. DOI: 10.1016/j.ijfatigue.2018.07.029.
- [15] A. U. Syed, F. D. Martinez, T. Roberts, et al., Performance comparison between isothermal hot corrosion and in situ cyclic hot corrosion of nickel-based superalloys. *Oxidation of Metals*, 2021. 96(1-2): 43-55. DOI: 10.1007/s11085-021-10044-9.
- [16] R. Pillai, A. Chyrkin, D. Grüner, et al., Carbides in an aluminised single crystal superalloy: Tracing the source of carbon. *Surface and Coatings Technology*, 2016. 288: 15-24. DOI: 10.1016/j.surfcoat.2015.12.066.
- [17] J. A. O'Brien, J. T. Hinkley, and S. W. Donne, Electrochemical oxidation of aqueous sulfur dioxide II. Comparative studies on platinum and gold electrodes. *Journal of The Electrochemical Society*, 2012. 159(9): F585-F593. DOI: 10.1149/2.060209jes.
- [18] K. L. Luthra, Low temperature hot corrosion of cobalt-base alloys: Part I. Morphology of the reaction product. *Metallurgical Transactions A*, 1982. 13A: 1843-1852. DOI: 10.1007/BF02647841.
- [19] M. Hellenbrandt, The inorganic crystal structure database (ICSD)-Present and future. *Crystallography Reviews*, 2004. 10(1): 17-22. DOI: 10.1080/08893110410001664882.
- [20] S. Gates-Rector and T. Blanton, The Powder diffraction file: a quality materials characterization database. *Powder Diffraction*, 2019. 34(4): 352-360. DOI: 10.1017/s0885715619000812.

- [21] Y. Wang, R. Pillai, E. Yazhenskikh, et al., Role of temperature in Na₂SO₄-K₂SO₄ deposit induced type II hot corrosion of NiAl coating on a commercial Ni-based superalloy. *Advanced Engineering Materials*, 2020: 1901244. DOI: 10.1002/adem.201901244.
- [22] K. A. Bol'shakov and P. I. Fedorov, Study of sodium sulfate-cobalt sulfate and sodium sulfate-nickel sulfate systems (In Russian). *Zhur. Obshchei Khimii* (Russian Journal of General Chemistry), 1956. 26.
- [23] W. Eysel, H. H. Hofer, K. L. Keester, et al., Crystal chemistry and structure of Na₂SO₄(I) and its solid solutions. *Acta Crystallographica Section B*, 1985. 41(1): 5-11. DOI: 10.1107/S0108768185001501.
- [24] E. Yazhenskikh, T. Jantzen, D. Kobertz, et al., Critical thermodynamic evaluation of the binary sub-systems of the core sulphate system Na₂SO₄-K₂SO₄-MgSO₄-CaSO₄. *Calphad*, 2021. 72: 122234. DOI: 10.1016/j.calphad.2020.102234.
- [25] Y. Wang, D. Sergeev, E. Yazhenskikh, et al., Experimental study coupled with thermodynamic assessment of the NiSO₄-K₂SO₄ quasi binary system. *Calphad*, 2021. 74: 102328. DOI: 10.1016/j.calphad.2021.102328.
- [26] D. Kobertz and M. Müller, Experimental studies on NiSO₄ by thermal analysis and calorimetry. *Calphad*, 2014. 45: 55-61. DOI: 10.1016/j.calphad.2013.10.008.
- [27] C. W. Bale, E. Bélisle, P. Chartrand, et al., FactSage thermochemical software and databases, 2010–2016. *Calphad*, 2016. 54: 35-53. DOI: 10.1016/j.calphad.2016.05.002.
- [28] E. Yazhenskikh, D. Sergeev, Y. Wang, et al., Critical thermodynamic evaluation of the system Na₂SO₄-NiSO₄. Under preparation.

- [29] A. Bellanca and P. di Mineralogia, L'afitalite nel sistema ternario K_2SO_4 - Na_2SO_4 - $CaSO_4$. *Periodico di mineralogia*, 1942. 13: 21-86.
- [30] K. L. Luthra and D. A. Shores, Mechanism of Na_2SO_4 induced corrosion at 600-900 °C. *Journal of The Electrochemical Society*, 1980. 127(10): 2202-2210. DOI: 10.1149/1.2129375.
- [31] R. A. Rapp and K. S. Goto. The hot corrosion of metals by molten salts. in *Proceedings of The Electrochemical Society*. 1981. DOI: 10.1149/198110.0159PV.
- [32] K. L. Luthra and O. H. Leblanc, Low temperature hot corrosion of Co-Cr-Al alloys. *Materials Science and Engineering*, 1987. 87: 329-335. DOI: 10.1016/0025-5416(87)90395-8.
- [33] T. Gheno, Gleeson, Brian, On the hot corrosion of nickel at 700 °C. *Oxidation of Metals*, 2015. 84(5-6): 567-584. DOI: 10.1007/s11085-015-9588-6.
- [34] B. Grégoire, X. Montero, M. C. Galetz, et al., Mechanisms of hot corrosion of pure nickel at 700 °C: Influence of testing conditions. *Corrosion Science*, 2018. 141: 211-220. DOI: 10.1016/j.corsci.2018.06.009.
- [35] E. Kistler, W.-T. Chen, G. H. Meier, et al., A new solid-state mode of hot corrosion at temperatures below 700 °C. *Materials and Corrosion*, 2019. 70(8): 1346-1359. DOI: 10.1002/maco.201810751.
- [36] H. Bei, E. P. George, and G. M. Pharr, Effects of composition on lamellar microstructures of near-eutectic Cr-Cr₃Si alloys. *Intermetallics*, 2003. 11(4): 283-289. DOI: 10.1016/S0966-9795(02)00251-0.
- [37] V. S. Stubican and R. C. Bradt, Eutectic solidification in ceramic systems. *Annual Review of Materials Science*, 1981. 11(1): 267-297. DOI: 10.1146/annurev.ms.11.080181.001411.

- [38] P. Waldner and A. D. Pelton, Thermodynamic modeling of the Ni-S system. *International Journal of Materials Research and Advanced Techniques*, 2004. 95(8): 672-681. DOI: 10.3139/146.018005.
- [39] L. A. Kochubei, E. V. Margulis, M. M. Shokarev, et al., The $\text{Al}_2(\text{SO}_4)_3\text{-K}_2\text{SO}_4$ system. *Russian Journal of Inorganic Chemistry*, 1978. 23(8): 1255-1257.
- [40] H. Du, Thermodynamic assessment of the $\text{K}_2\text{SO}_4\text{-Na}_2\text{SO}_4\text{-MgSO}_4\text{-CaSO}_4$ system. *Journal of Phase Equilibria*, 2000. 21(1): 6-18. DOI: 10.1361/105497100770340363.


Declaration of interests

The authors declare that they have no known competing financial interests or personal relationships that could have appeared to influence the work reported in this paper.

The authors declare the following financial interests/personal relationships which may be considered as potential competing interests:



Click here to access/download
Supplementary Material
Supplementary 1_DTA result.docx





Click here to access/download

Supplementary Material

Supplementary 2_Phase equilibria (log pSO₃=-3.79,
T=700C).TXT